ABSTRACT

Title of Thesis: CHARACTERIZATION OF NON-DISPERSIVE INFRARED SENSORS FOR R-32 AND R-454B LEAKS

James Leahy, Master of Science, 2022

Thesis Directed By: Professor Peter B. Sunderland, Department of Fire Protection Engineering

Due to the increased concerns about climate change, multiple states including California have started to pass legislation that phases out high global warming potential (GWP) refrigerants in HVAC and refrigeration systems. The likely replacements are A2L refrigerant which have lower GWP and are mildly flammable. This will require area monitoring leak detection systems for all future applications of these refrigerants. These detection systems preferably need to operate continuously for up to 15 years. The UL 60335-2-40 (2019) standard defines the sensor response time which must alarm within 10 seconds of exposure to 100% of the refrigerant's LFL. Development of sensors capable of meeting the UL 60335-2-40 standard has been slow with many different types of gas sensing technologies being used. One of these technologies that was identified as a potential candidate was non-dispersive infrared (NDIR). A sensor not yet available commercially was able to be obtained to test its response to A2L refrigerants R-32 and R-454B according to the UL 60335-2-40 standard. Three other competing sensing technologies were also obtained to compare the performance of other sensors about to hit the market. These sensors were characterized by their linearity to varying concentrations of A2L refrigerant, response time, and to contamination. All the tested sensors were able to meet the 10 second requirement for response

time. However, all but the NDIR sensor experienced a change in output when exposed to a list of prescribed contaminants by the UL 60335-2-40 standard. After the contamination, the NDIR sensor showed no change in its output indicating it experienced no poisoning effect. The NDIR sensor was deemed to have the optimal performance out of the sensing technologies. Long term exposure, exposure to contaminants and refrigerant at the same time, and service lifetime are still concerns.

CHARACTERIZATION OF NON-DISPERSIVE INFRARED SENSORS FOR R-32 AND R-454B LEAKS

by

James Leahy

Thesis submitted to the Faculty of the Graduate School of the
University of Maryland, College Park, in partial fulfillment
of the requirements for the degree of
Master of Science
2022

Advisory Committee:
Professor Peter B. Sunderland, Chair
Professor James A. Milke
Professor Arnaud C. Trouvé

Acknowledgments

I would like to start by thanking Dr. Peter Sunderland. He is the reason that I first got involved in the project as an undergraduate and encouraged me to become a Master of Science student. I could not have seen myself being able to achieve my academic accomplishments without his support. Dr. Sunderland was a very erudite advisor, and was able to provide constructive feedback in a very positive way. Dr. Sunderland was also very understanding and patient mentor when it came to matters outside of school. For all these reasons, I am grateful to have had you as my advisor and strive to have the same attitude you do towards both work and life.

Next, I want to thank Carrier who gave me the opportunity to obtain a master's degree by supporting me and my research financially. Marcin Piech and Michael Birnkrant were the two in charge of the project, and they were always readily available to meet and answer any questions I had. You both made working on this project a stress free and an enjoyable experience for me, and I am grateful to have been given the opportunity to work with you.

I would also like to extend my gratitude to the FPE faculty and students who were a part of my academic journey. To John Hoffman, Joe Alascio, Garrett Wack, and Chris Chen who all worked on the project with me at varying times and made themselves available to me as a resource even when they had moved on from the project. To Fernando Raffan-Montoya who managed the lab spaces I worked in and helped me when I had questions about procedures in the lab. To all my teachers and classmates who provided me a positive learning experience throughout both my undergraduate and master's degree. To my Master of Science and undergraduate advisors, Arnaud Trouvé and Nicole Hollywood, who was very supportive of my pursuit of my master's degree.

Both of you were very helpful and available even while school was virtual only due to the pandemic. And to Dr. Milke and Dr. Trouvé for serving on my thesis committee.

Lastly, I would like to thank all my family and friends who supported me at home. To all my friends who provided many fun conversations and activities even while we were all stuck at home. To my parents who have supported me my whole life. It is thanks to your help that I have gotten to where I am today, and your continued support is part of the reason I have succeeded thus far. And lastly to my fiancé, who has always supported me since I have known her. I am grateful that I have the opportunity to support you as well for the rest of our lives.

Table of Contents

List of Tables

List of Figures

Chapter 1: Introduction

1.1 Motivation

Due to the increased concerns about climate change, multiple states including California have started to pass legislation that phases out high global warming potential (GWP) refrigerants in HVAC and refrigeration systems. Currently, these HVAC and refrigeration systems typically use hydrofluorocarbons (HFCs). HFCs are non-flammable and are not very toxic. HFCs do have large GWP values usually ranging from 1,430 to 3,985 [1]. Due to the continued effects of climate change, legislation is now requiring that another lower GWP refrigerant be used for these systems.

These alternative refrigerants with much lower GWP values are called A2L refrigerants. A2L refrigerants are mildly-flammable but have a GWP range between 4 and 675 [2]. This classification of refrigerant was created by ASHRAE. The A2L classification means that the refrigerant meets the lower flammability classification (A2), but has a burning velocity equal to or greater than 10 cm/s tested at standard temperature and pressure [3]. These refrigerants can be pure HFC-32 or HFC-32 blended with HFO-1234yf or HFO-1234ze [4]. The refrigerant classification for all classes of refrigerants can be seen summarized in Table 1.1.

California intends to stop the use of refrigerants with a GWP value greater than 750 for commercial and residential HVAC and refrigeration systems by as soon as 2023 [6]. A2L refrigerants fit this requirement, however they do pose a fire hazard. Therefore A2L area monitoring leak detection systems are needed as a preventative measure to this hazard.

The availability of A2L refrigerant area monitoring sensors for residential use is limited because of their expensive prices. Currently A2L sensors that are used outside of residential

applications cost thousands of dollars. The hope is that once a viable solution is identified, mass production will drop the cost of the sensor to around $10. Ideally this sensor would not need any maintenance for 15 years. The UL standard 60335-2-40 [7] details that the sensor must respond within 10 seconds of being introduced to a concentration of 100% of the refrigerant's lower flammability limit (LFL), as described in Annex LL, Section 3. Section LL.3DV describes a state of health test which must be performed on the sensor after the contaminant test. It requires that the sensor show no signs of poisoning after being exposed to the contaminants [7]. Sensors capable of meeting these standards have been slow to develop. Today sensors are either just starting to hit the market or are very close to it. It is important to characterize these sensors' response to determine their viability for A2L area monitoring leak detection.

Table 1.1. Refrigerant classification, reproduced from [5].

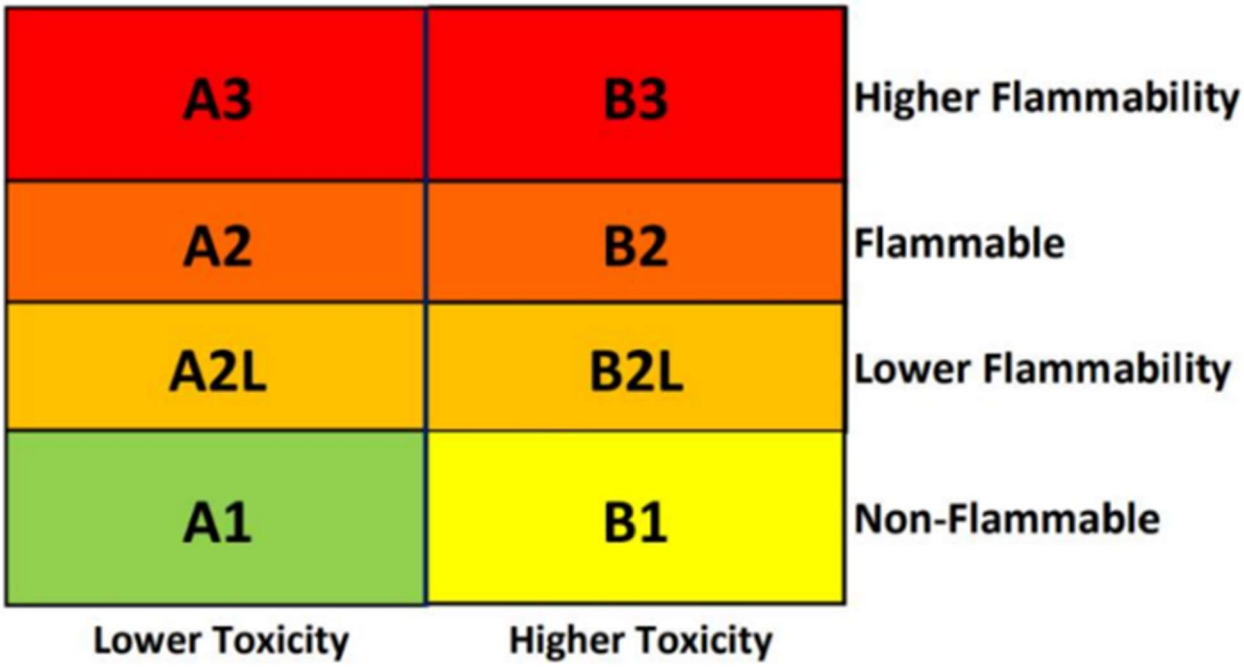

1.2 Literature Review

This literature review was conducted in order to learn more about available sensing technologies in order to choose an appropriate sensor for the purposes of this study. A list of available gas sensing technology was compiled for review. This list was then cut down to the sensing technology that could possibly meet the goals of this study. The chosen technology was then further reviewed to understand the science and engineering behind the sensors. Lastly, a list of sensors of the chosen technology were compiled and compared to make a final selection for testing.

1.2.1 Comparison of Available Sensing Technologies

McClure and Anderson [8] reviewed possible area monitoring sensing technologies that would reduce costs and losses after a regulation that required CFC production to be cut down by 50%. The technologies they reviewed were gas ionization, metal-oxide semiconductor (MOS), and infrared (IR). McClure and Anderson [8] concluded that the MOS technology is the optimum method for monitoring smaller rooms due to its low cost. However, they recommend the IR technology for its ability to be highly specific and shield out other gasses that could give false alarms to MOS. and gas ionization. Tapscott and Sohn [9] prepared a list of halocarbon refrigerant detection technologies for the U.S. Army Corps of Engineers. This list was compiled in order to help the U.S. Army replace current high GWP refrigerants that the U.S. army used in preparation for the eventual transition away from high GWP refrigerants. They did this by using Tapscott and Sohn's list to determine a suitable sensing technology that could detect low GWP refrigerants.

Tapscott and Sohn's list is summarized in Table 1.2. The sensing technologies in this list can be categorized into three classifications of selectivity. These classifications are non-selective,

halogen-selective, and compound selective sensors. Nonselective sensors are able to detect many gasses, including gasses that are not refrigerants. Halogen-selective sensors are only able to detect compounds that contain a halogen atom. Compound-selective sensors are ones that are calibrated to detect a predetermined compound [9].

Tapscott and Sohn [9] also suggest that as sensors get more selective, they cost and complexity also increase. Due to the sensor requirements of meeting UL standard 60335-2-40 [7], the compound-specific selectivity sensors should be further examined as a potential candidate sensing technology. Tapscott and Sohn [9] state that gas chromatography sensors are widely available and could be used for area monitoring in theory, but have not been used much for refrigerant detection. Infrared sensors are commonly used for area monitoring. IR sensors also have a high sensitivity and can be calibrated to detect a specific compound without interference from other gasses. The downside of IR sensors is that they tend to be the most expensive of the available sensors. Mass spectra-based sensors are capable of being highly specific by programming the sensor to scan for specific mass peaks. However, this technology is the most expensive, uses very sensitive equipment for operation, and requires high levels of maintenance/upkeep [9].

Tapscott and Sohn [9] summarize that negative corona discharge sensors are the best option for pinpointing leaks. This study's purpose is to test an area monitoring sensor, so this sensor was not considered for testing. For area monitoring, Tapscott and Sohn [9] state that solid state and infrared sensors are the best options. Solid state sensors are a cheaper option when compared to infrared sensors, but are not able to perform well when interference from other gasses need to be considered. While infrared sensors are more expensive, they excel in performance when selectivity needs to be considered. While Tapscott and Sohn [9] have presented a thorough comparison of

available detection technologies, the list is over 25 years old and these sensing technologies have advanced considerably.

Table 1.2. Commercially available refrigerant sensing technologies. Reproduced from [10].

Technology	Principle
Nonselective	
Flame ionization	Gas is pulled into a hydrogen flame. Ionized gas is detected with an electrode. Gasses with carbon will emit a signal.
Gas-membrane galvanic cell	Gas is pyrolyzed by a hot filament. Product passes through a membrane and is absorbed onto an electrode. Redox reaction on counter electrode results in a current equivalent to gas concentration.
Negative corona discharge	Two electrodes are exposed to atmosphere in a housing. Housing becomes ionized. Gas changes the dielectric breakdown potential. Resulting current change creates signal.
Solid state	Gas changes the resistivity of heated metal-oxide semiconductor.
Thermal conductivity	Gases conduct heat differently than air. Contaminants are identified from thermal conductivity of mixture.
Halogen-Specific	
Electron capture	Radioactive source creates electron flow. Gas enters sensor and removes electrons from flow. Decrease in current activates signal.
Heated diode	Gas is thermally decomposed. Halogen atoms react with alkali metal atoms. Resulting ion current measures concentration of gas.
Compound-Specific	
Gas chromatography	Gas mixture is separated. Individual components are identified.
Infrared (IR)	Beam of infrared radiation is passed through gas. Absorption is determined at selected wavelengths.
Mass spectra-based	Gas is scanned for specified mass peaks to identify a certain gas.

Wagner and Ferenchaik [5] present a more modern comparison of refrigerant sensing technologies. Based on their review of refrigerant sensing technology, the list of presented technologies in Table 1.2 can be narrowed down to Infrared, Electrochemical Cell (EC), metal oxide semiconductor based solid state sensors, and heated diode sensors. Wagner and Ferechaik [5] came up with a failure mode ranking based on ways that the sensor could potentially fail in varied settings. This failure mode ranking system is presented in Table 1.3 [5]. Wagner and Ferechaik [5] assign a score to each sensor technology on the basis of likelihood and severity of the proposed failure modes. The higher the score of the sensor, the higher the impact will be on the sensor's ability to operate. These proposed failure modes and their corresponding ranking score are reproduced in Table 1.4 and 1.5 [5] for commercial/industrial and residential applications.

Table 1.3. Failure mode scores, reproduced from [5].

Likelihood		Severity				
		Not Applicable (NA)	Low (L)	Moderately Low (ML)	Moderately High (MH)	High (H)
	Not Applicable (NA)	0	-	-	-	-
	Unlikely (U)	-	2	3	4	5
	Moderately Unlikely (MU)	-	3	4	5	6
	Moderately Likely (ML)	-	4	5	6	7
	Likely (L)	-	5	6	7	8

Table 1.4. Failure mode scores for commercial/industrial applications, reproduced from [5].

Failure Mode		IR		EC		MOS		Catalytic		Heated Diode	
Humidity	Likelihood	U	3	MU	5	U	4	U	2	L	7
	Severity	ML		MH		MH		L		MH	
Temperature	Likelihood	U	3	U	3	MU	4	MU	3	U	2
	Severity	ML		ML		ML		L		L	
False Triggering Gases	Likelihood	NA	0	ML	6	ML	5	NA	0	ML	5
	Severity	NA		MH		ML		NA		ML	
Poisoning or Blocking Gases	Likelihood	ML	4	ML	6	U	2	ML	5	NA	0
	Severity	L		MH		L		ML		NA	
Overexposure	Likelihood	U	2	L	6	ML	5	ML	5	ML	5
	Severity	L		ML		ML		ML		ML	
Air Contaminants	Likelihood	U	3	U	2	MU	3	MU	3	U	2
	Severity	ML		L		L		L		L	
Total		**15**		**28**		**23**		**18**		**21**	

Table 1.5. Failure mode scores for residential applications, reproduced from [5].

Failure Mode		IR		EC		MOS		Catalytic		Heated Diode	
Humidity	Likelihood	U	3	U	4	U	4	U	2	U	4
	Severity	ML		MH		MH		L		MH	
Temperature	Likelihood	U	3	U	3	U	3	U	2	U	2
	Severity	ML		ML		ML		L		L	
False Triggering Gases	Likelihood	NA	0	MU	5	U	3	NA	0	MU	4
	Severity	NA		MH		ML		NA		ML	
Poisoning or Blocking Gases	Likelihood	MU	3	ML	6	U	2	ML	5	NA	0
	Severity	L		MH		L		ML		NA	
Overexposure	Likelihood	U	2	U	3	U	3	U	2	U	3
	Severity	L		L		L		L		ML	
Air Contaminants	Likelihood	U	3	U	2	MU	3	MU	3	U	2
	Severity	ML		L		L		L		L	
Total		**14**		**23**		**18**		**14**		**15**	

Each sensor technology had a lower failure mode score in the residential application setting. The IR sensors had the lowest scores in both the residential and the commercial/industrial application. Wagner and Ferechaik [5] summarize that the IR sensors score the best because of their ability to operate under a wide range of environmental conditions, and are not affected by false alarm gasses, over-exposure, or air contaminants because of their air filter. Heated diode sensors had the second-best score of the four sensors in question. The heated diode sensor had issues failing due to humidity conditions and false alarms, but not to contamination. EC sensors had the highest failure mode score for both of the specified settings. Wagner and Ferechaik [5] summarized that this was because of the likelihood of over-exposure and moderately high impacts of false-triggering gasses. MOS solid state sensors had the second highest failure mode score of the four sensing technologies. Wagner and Ferechaik [5] state that the MOS solid state sensors suffer from drift due to over exposure to refrigerants and are susceptible to cross sensitivity.

Wagner and Ferechaik [5] made the conclusion that MOS solid state and IR sensing technology would be the most practical options. EC sensors were determined to be too susceptible to the proposed failure methods by Wagner and Ferechaik [5]. Heated diode technology has the potential to be adapted for A2L refrigerant detection, but are currently not being manufactured to detect A2L refrigerants.

Wagner and Ferechaik [5] determined that MOS sensors would be the most practical for residential application due to not being highly susceptible to most failure modes within residential applications and are already available on the market at low costs. The issue would be the required annual maintenance. The IR sensors were considered most practical for commercial/industrial settings because they were least susceptible to failure modes within the commercial/industrial setting. Maintenance on the sensor would be less of a problem here because technicians could

regularly check on the sensors. The price point for IR sensors is much higher than MOS solid state sensors. However, Wagner and Ferechaik [5] stated that IR sensor manufacturers have indicated that the sensors could be adapted for the residential setting at a much lower cost. Wagner and Ferechaik [5] also stated that MOS sensors could be used for commercial/industrial applications, but the susceptibility to contamination and effects of over-exposure would have to be addressed.

Danfoss is a prominent figure in refrigerant gas sensing technologies. They have an application guide [11] that talks about the sensing technologies that they sell: MOS solid state, EC, catalytic, and IR. Table 1.6 [11], reproduced from Danfoss, shows which of the sensing technologies are suitable for A2L refrigerant detection. The EC sensors were deemed suitable only for ammonia. The catalytic sensors were deemed unsuitable due to effects from poisoning. Only the MOS solid state and IR technologies were deemed suitable for A2L sensing, with MOS solid state being the preferred solution.

Table 1.6. Sensor suitability to a given refrigerant, reproduced from [11].

	Semi-conducter	Electro-chemical	Catalytic	Infrared
Ammonia "low" concentration (< 100 ppm)	–	✔	–	–
Ammonia "medium" concentration (< 1000 ppm) [1])	(✔)	✔	–	(✔)
Ammonia "high" concentration (<10000 ppm)	✔	–	✔	(✔)
Ammonia "very high" concentration (> 10000 ppm)	–	–	✔	(✔)
Carbon Dioxide CO_2	–	–	–	✔
HC Hydrocarbons	(✔)	–	✔	(✔)
HCFC - HFC Halocarbons	✔	–	–	(✔)

✔ Best solution (✔) Suitable - but less attractive – Not suitable

Fig. 4

With the recent changes to the UL 60335-2-40 [7] standard, many new types of sensors using emerging technologies have started to be produced. NevadaNano has recently trademarked a new type of technology that they call molecular property spectrometer (MPS). The way that NevadaNano describes the technology is an integration of many chemical sensors onto a single silicon chip.

> "The chip incorporates a patented array of micro-cantilevers with integrated piezoelectric sensing elements that provide electrical actuation and sensing of resonance frequency. Monitoring resonance is a highly sensitive way to measure very small masses of adsorbed analyte. An array of sensors can be electrically monitored in a low-cost, robust fashion because of the unique piezoelectric configuration the MPS allows. Whereas, the more common alternative of using an optical readout is more expensive but less robust." [12]

However, since this technology was only recently developed by NevadaNano, it has not yet been compared and contrasted with existing sensing technologies like Danfoss [11] has done. Another type of emerging gas sensing technology is the thermal conductivity sensor. This type of sensor is a popular choice used in gas chromatography. The sensor consists of a metal filament that is heated up. This causes small changes in the thermal conductivity of vapors surrounding the sensor. This change in thermal conductivity is proportional to the amount of those vapors present around the sensor [13]. The last identified emerging gas sensing technology were speed of sound (SS) sensors. These sensors operated by measuring the change in the speed of sound inside a resonant cavity. These sensors can either use the time-of-flight method in which the amount of time an emitted pulse takes is measured, or the shift in resonance frequency method [14]. All three of these sensing technologies are currently being used to develop A2L gas sensors.

1.2.1.1 Selection of Sensing Technology

After reviewing the previous literature, the chosen refrigerant detection technology was IR sensing. MOS solid state sensing is a cheaper alternative that is already on the market for residential applications. They are also able to last for a long time, but contamination from other gasses and the effects from over-exposure to refrigerants make the sensor too much of a burden to leave in residential applications. IR sensors do not suffer from contamination effects or over-exposure to refrigerants. Currently, the IR sensors are a more expensive option than MOS solid state sensors. If the technology is found more suitable to the requirements for A2L detection then it is likely that manufacturers will start offering sensors adapted for residential applications at more comparable costs to the MOS solid state sensors.

1.2.2 Introduction to IR Technology

IR sensors [15] [16] [17] have widespread applications for both academic, government, business, industrial, and many more fields. Common uses include air-quality monitoring, greenhouse farming, and industrial process control [15]. This is mostly due to the ability to preprogram these sensors to sense specific compounds with high accuracy. IR sensors are suitable for the detection of many gaseous pollutants including hydrogen fluoride pollutants [17]. IR sensors use a technique called infrared spectroscopy. This is a method of obtaining an infrared spectrum by passing infrared radiation through a sample and measuring how much of the incident radiation was absorbed [17]. Non-dispersive infrared (NDIR) sensors were developed in the 1930's that applied infrared spectroscopy to measure gas concentration [17]. To understand how the gas

concentrations are measured, first the Beer-Lambert law should be examined shown in equation 1 [15] [16]:

$$I\lambda = I_0\lambda \exp(-kcL). \quad (1.1)$$

In equation 1.1, Xu et al [16] explain that λ is the wavelength of the incident light in mm, c is the concentration in ppm, k is the correlation coefficient of gas absorption, and L is the optical path length in mm. I is the measured light intensity at the end of the optical path L, I_0 is the initial light intensity emitted at the beginning of the optical path. This k value is specified based on the properties of the target gas. Based on this equation, it can be rewritten as the transmission T of initial light intensity, I_0 to the end of the length L shown in equation 2 [15]

$$T = I/I_0 = \exp(-kcL). \quad (1.2)$$

Under the assumption that a sensor has a fixed optical path length, equation 1.2 shows that the transmission is directly related to the gas concentration. This method allows for sensors to identify specific gasses based on their wavelength absorption.

During the detection, it is likely that the target gasses are surrounded by dust particles or water vapor which can absorb infrared light and skew the detection results [18]. Y. Jing et al. [19] have further modified the Beer-Lambert law to correct for dust and water vapor interference with

$$T(\lambda, L) = I_0\lambda \exp(-\alpha\lambda PcL + m\lambda L + n\lambda L + \varepsilon_w\lambda L). \quad (1.3)$$

Equation 1.3 shows the modified Beer-Lambert law where $\alpha\lambda$ is the absorption coefficient of the infrared light, P is pressure, $m\lambda$ is the Raleigh scattering coefficient, $n\lambda$ is the Mie scattering coefficient, and $\varepsilon_w\lambda$ is the absorption coefficient of water [19].

NDIR sensors use two inputs to detect the concentrations of target gasses. The other method for detecting gas concentration is by a change in temperature [19]. When the infrared radiation interacts with the gas molecules, the energy from the radiation that has the same wavelength as the natural frequency of the gas molecule gets absorbed by that molecule. This in turn causes the molecule to start vibrating at a higher frequency and results in an increase in temperature [19]. This temperature increase is proportional to the gas concentration and can be detected by NDIR sensors.

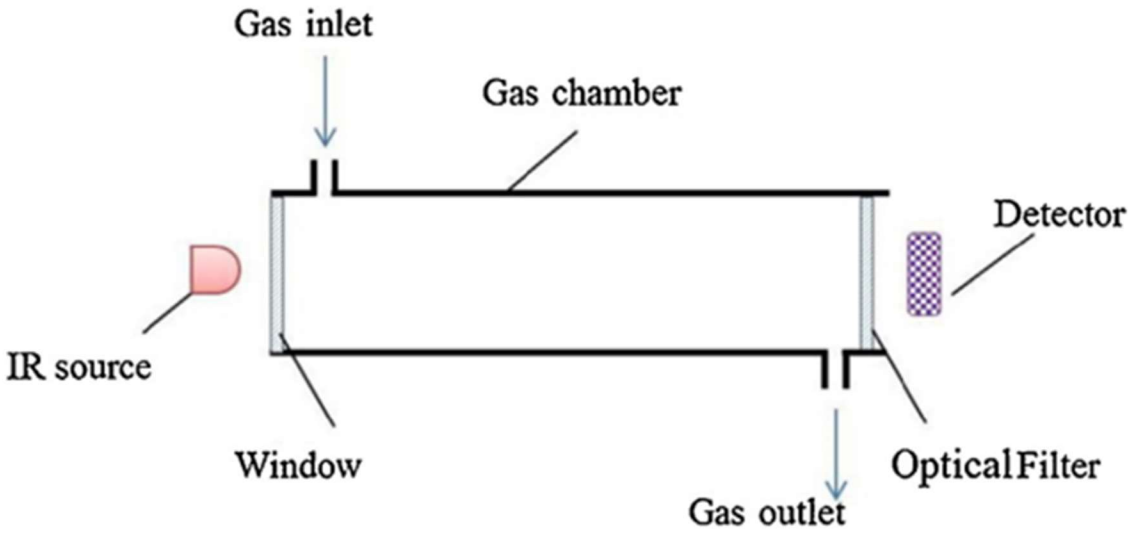

Figure 1.1 Simple design for a typical NDIR sensor. Reproduced from [17].

The sensitivity of the sensor is largely affected by the design of the sensor. A simplistic design of a typical NDIR sensor is shown in Figure 1.1. The sensor has three key parts including the IR source, optical gas chamber, and the detector. Two types of IR light sources typically get used in NDIR sensors [20]. The first light source is the collimated style. This style of IR light

source projects most of the IR light directly onto the detector and has a larger range of gas detection [20]. The divergent IR light source is emitted in all directions and cannot be accurately projected onto the detector [20]. The optical gas chamber can be tuned to fit the needs of the sensors. The parameter for the optical gas chamber is the optical path length [19]. The optical filter inside the gas chamber is selected to allow transmission of the desired wavelength [19]. The gas chamber needs to be filled with inert gasses to protect the life span of the sensor. Sklorz et al [18] found that using a conical gas chamber and fresnel lenses produced the best incident radiation intensity. An increase in the signal intensity meant an increase in measurement efficiency [18].

Y. Jing et al. [19] state that NDIR sensors typically use six different types of detectors. These detectors include thermoelectric, thermistor bolometer, pyroelectric detector, photon detector, luft detector, and photoacoustic detector [19]. However, the pyroelectric detector is the most commonly used detector. This is because pyroelectric detectors use materials made from crystals which experience spontaneous polarization [19]. This is a phenomenon where the crystal develops an electrical charge that is directly dependent on the temperature [19]. The temperature is dependent on the intensity of the incident radiation. As the radiation reaches the surface of the detector, an electrical current is induced by the change in temperature [19]. Along with good stability and a responsiveness to many wavelengths make this detector a popular choice.

NDIR sensors have an advantage over other types of spectroscopy technologies. The NDIR sensor requires little energy to run [17]. This allows for IR wavelengths between 1 - 15 micrometers to operate at much lower temperatures than other sensors. This can be seen in Figure 1.2.

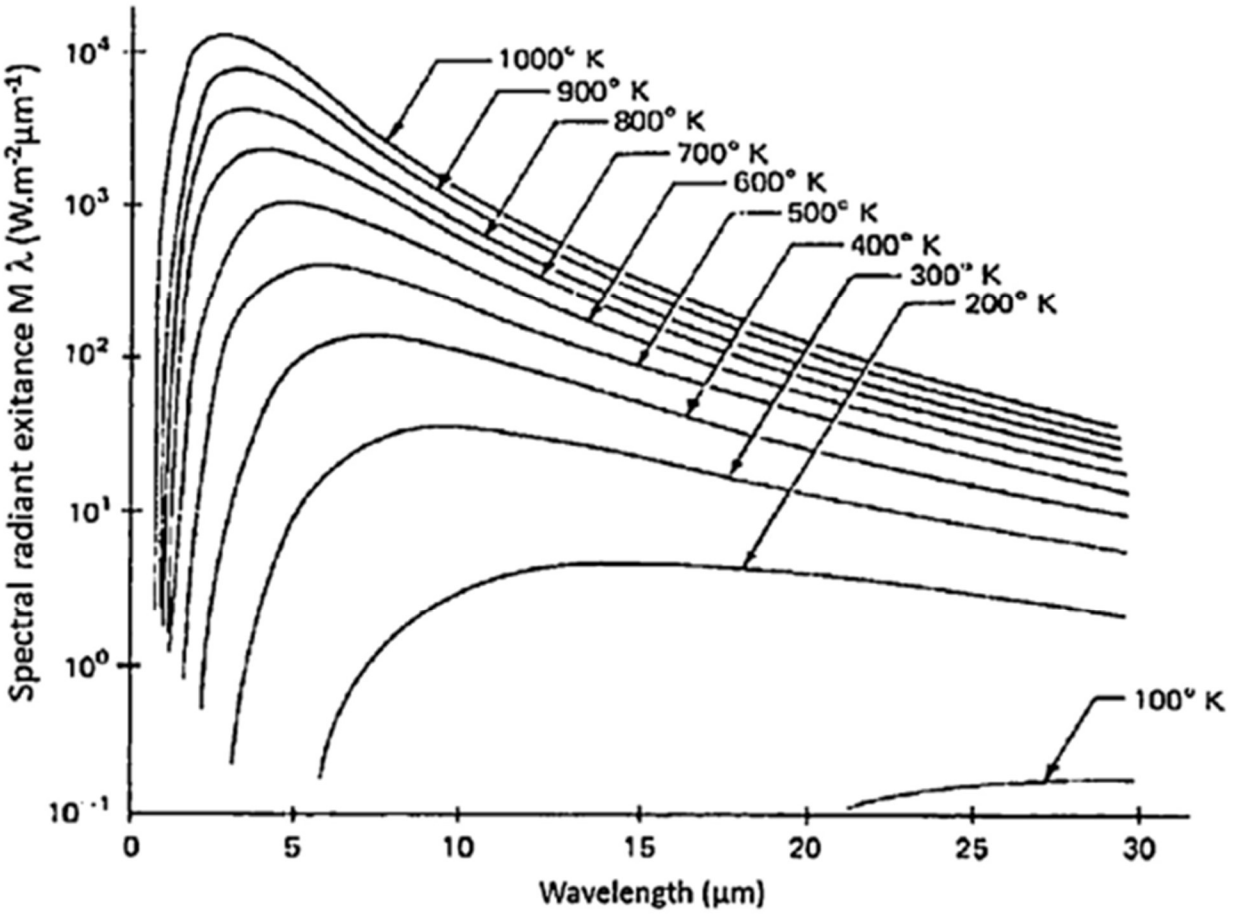

Figure 1.2 Relationship between the temperature of blackbody and the wavelength of radiation. Reproduced from [17].

1.2.3 Comparison of Available NDIR Sensors

There is an abundance of commercially available NDIR sensors that are available on the market, all with varying prices, sizes, and intended uses. The vast majority of these sensors on the market are intended for indoor air quality monitoring through the detection of CO2. Because the need for area monitoring sensors capable of detecting A2L refrigerants has only recently begun to be needed, there are few to no commercially available NDIR sensors designed for A2L refrigerants.

There are companies like SenseAir and NET that are working to develop a sensor for the market that can meet all the emerging standards.

Some companies have released a sensor like the Cubic CU-AM4205 as seen in Figure 1.3. This sensor is advertised to have an over 15 year life span and uses industry standard serial UART and analog output. It can measure between 0-50% of the LFL with an accuracy of 3.75% LFL. The sensor is already calibrated to its target gas which is R-32. The CU-AM4205 is available for $99 [21].

Another company which has plans to release a lineup of NDIR gas leak sensors for A2L gasses is N.E.T. This company has a lineup called the IREF LITE series. These sensors will be capable of detecting a multitude of different A2L gasses including R-1234yf, R-32, R-454b, and several others. The detection ranges from 5,000 ppm to 10,000 ppm depending on the target gas. Other companies that are currently working on developing their own sensors include Amphenol, GORE, and PST.

Figure 1.3. Commercially available NDIR A2L sensor. Reproduced from [21].

1.2.3.1 Selection of Sensor

The selected sensor is not yet released commercially yet. Due to the competitive nature of the development of NDIR sensors capable of detecting A2L refrigerants, the sensor will not be named. However, the selected sensor acquired from Company X using NDIR technology can detect the necessary range for the new standard, as well as sufficient for testing various concentrations above and below the required concentration. Since the sensor has not been released yet, the price cannot be determined. However, it will likely be competitive with other market prices such as the Cubic CU-AM4205 at $99. The sensor is also capable of serial UART and analog output making data collection simple. Multiple versions of the sensor provided by Company X were acquired for testing. In addition to this sensor, the MPS, thermal conductivity, and SS sensors were also acquired to characterize and compare their response to A2L refrigerants with the NDIR sensor.

Table 1.7. Selected sensors for testing.

Sensor	Technology
NDIR	Non-dispersive Infrared
MPS	Molecular Property Spectrometer
SS	Speed of Sound
TC	Thermal Concuctivity

1.3 Objectives

The objective of this study is to determine a viable sensing technology such that A2L refrigerants can be used in HVAC and refrigeration systems. First, a sensing technology needs to be identified as a potential candidate for A2L area monitoring. Then an apparatus must be designed and built to facilitate these tests. In these tests, two sensor performances were measured. One of these performances was the sensor's response to 100% of the LFL of the A2L refrigerants. The goal of

this test was to measure a defined response within 10 s. The two A2L class refrigerants chosen for this test were R-32 and R-454B. The second sensor performance measured was the response from exposure to a prescribed concentration of contaminants. This chosen list of contaminants are ones commonly found around a household and may become airborne.

A literature review was conducted to determine and compare possible sensing technologies for A2L area monitoring applications. One of the options determined from this literature review was nondispersive infrared (NDIR) sensors. NDIR sensors not yet available commercially were obtained and used for testing. Other emerging A2L sensors using MPS, thermal conductivity, and SS technology were also acquired to compare sensor performances. The apparatus built for testing was designed so that a mixture of air and refrigerant/contaminant could be delivered at desired concentrations. Multiple calibrations were performed on the test apparatus to ensure that the expected concentration was as close to the actual concentration as possible. The sensors were then characterized according to their sensitivity/response time, time to recover, and contaminant response.

The objectives of this study are:

- Determine an available sensing technology and a corresponding sensor available for purchase
- Construct an apparatus to test with this sensor
- Determine the sensors response time to A2L class refrigerants, R-32 and R-454B
- Determine the sensors response to contaminants and contaminant effect on sensor health

Chapter 2: Experimental

2.1 Sensor Specifications

Due to the proprietary nature of the development and marketing of A2L refrigerant sensors, specifics cannot be given. However, a general description of the sensor can be provided. The sensor acquired from Company X uses NDIR technology in conjunction with a pyroelectric detector to capture concentrations of hydrocarbons, CO2, and refrigerants. Specifically, this sensor best measures gas concentrations of 0% - 100% LFL for hydrocarbons, R1234yf, R1234ze, and R32. The optical path of the sensor uses a metal that has been treated to stop oxidation and promote brightness. The sensor operates between -40 and 60 C and within 0 - 95% humidity. The sensor also comes calibrated with a temperature compensation report included in the manual. The sensor also weighs about 40 grams and is 32 mm in diameter [22]. An image of the sensor can be seen in Figure 2.1.

Figure 2.1. Image of the housed NDIR sensor provided by Company X.

The sensor runs on a voltage between 3.5 Vdc - 5.5 Vdc. The sensor has a 5-pin connection which can provide either an analogue or digital output. The analogue output is a voltage signal that is linearized, and temperature compensated between 0.4 Vdc - 2 Vdc. This is capable of being customized by the customer. The digital output is in the universal asynchronous receiver-transmitter (UART) protocol format. UART is a serial communication interface that allows for serial data to be received and transmitted remotely using a modem connected to a serial port [23]. This method of data acquisition allows for data to be gathered by a data logger and accessed remotely at any time. A graphic of the UART protocol can be seen in Figure 2.2.

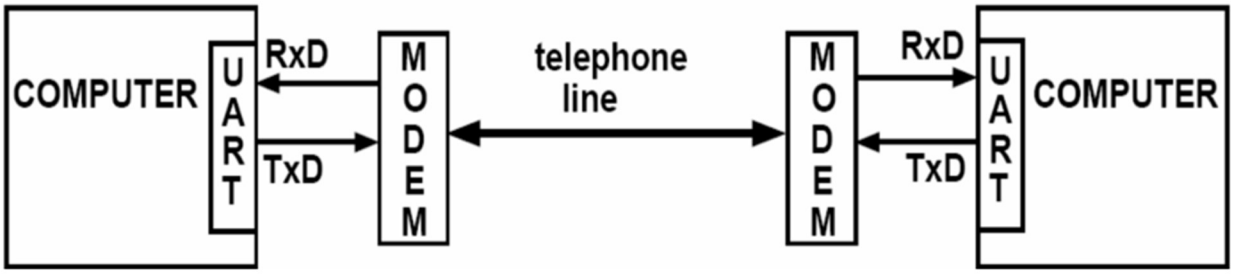

Figure 2.2. UART protocol serial data transmission. Reproduced from [23].

The MPS sensor uses a micro-machined membrane with a heater and thermometer that measures changes in the thermodynamic properties of the gas mixture. It weighs about 8 grams and has the dimensions 0.65 x 0.79 inches. It operates on 3.3 Vdc – 5.0 Vdc and outputs to UART or I2C protocols on a 4 – 5 pin connection. It can operate it temperatures from -40 – 75 C in a humidity range up to 100% RH.

The TC sensor operates using a gas permeable membrane that protects a thermometer probe. This probe measures temperature and flow characteristics of the gas mixture when exposed to a heater. It had a volume of 10.1 x 10.1 x 6.5 mm^3. It had a 5 pin connection and outputted to

UART and I2C. It operates on a voltage between 2.4 Vdc and 5.5 Vdc. The operating temperature range is -10 – 60 C and the humidity range was up to 95% RH.

The SS sensor measures changes in the speed of sound in a resonant cavity using a piezoelectric sensor. It has a diameter of 24 mm and is 18 mm deep. It operates on 2.4 Vdc – 5.0 Vdc and outputs data using the UART and I2C protocols.

2.2 Sensor Setup

Before the sensor could start outputting data, a list of items was required. First was a power supply, a data logger capable of using the UART protocol, and an internet connection. The power supply used was a Mean Well LPV-60-12 box type enclosed power supply. It could provide up to 12 V of AC or DC voltage with up to 5 A of current. This power supply was used to provide power to the data logger. The data logger was supplied by Carrier Corp. and was independently developed. The data logger had 12 UART serial ports, 12 input/output (I/O) ports, and 2 RS-485 ports. Each port was able to be configured remotely to the specification of whichever sensor was going to be using that port. Only the UART serial ports were used to test the NDIR sensor. Figure 2.3 depicts the power supply and data logger used. For connection to the internet, a Netgear Nighthawk wireless mobile router was used. This allowed for remote communication and access to the data logger.

Connecting the sensor to the data logger was very straight forward. The sensor came ready to be plugged into the UART ports and the ports were remotely configured to the specifications of the sensor. As soon as the sensor was connected to the datalogger, it would start recording data which would be saved and logged in the data cloud. This data cloud could be accessed at any time

to retrieve the data of interest. In the case of a power outage, the data logger also came with a USB port and an empty USB stick which would record data until the data logger could communicate wirelessly again. Figure 2.4 shows a visual schematic of the data logging and wiring arrangement.

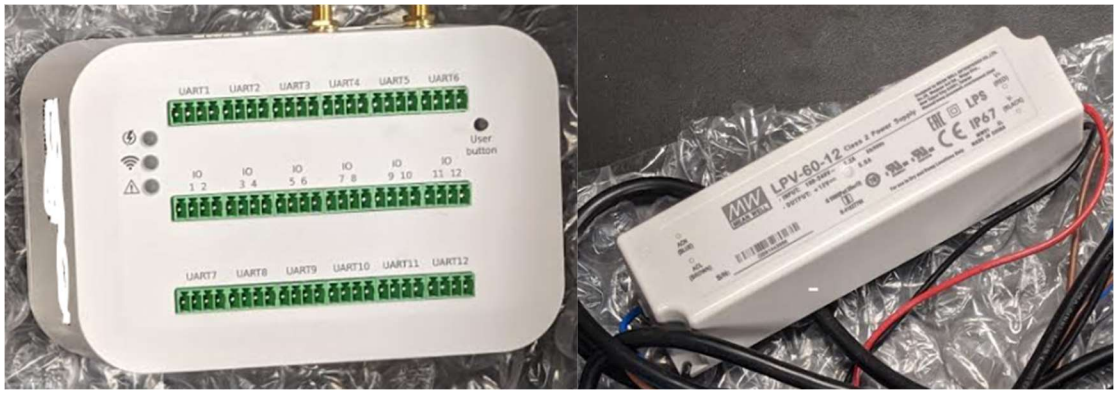

Figure 2.3. Data logger (left) and power supply (right) used.

To retrieve the output of the sensor, the data had to be accessed via the data cloud. Once in the data cloud, the data logger used was selected. The data cloud had an export feature. This feature was activated by selecting the export data button clearly displayed in the data cloud. This feature allows you to choose a time window for export, as well as which sensors you would like to export data from. The data was exported as an excel file. As the data logger was always recording, there were no procedures for initiating the data logger. Only marking the time of the beginning and end of the test was necessary. This made testing multiple sensors at the same time convenient.

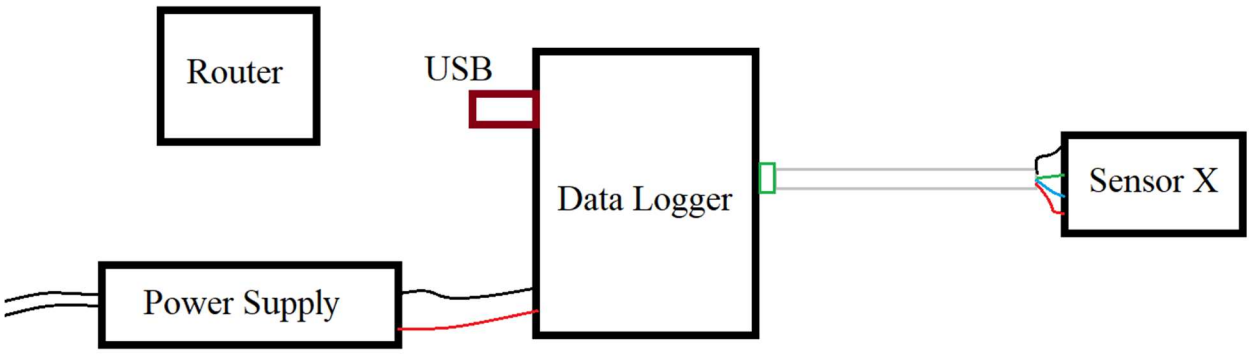

Figure 2.4. Data logging and wiring diagram.

2.3 Test Apparatus

This section describes the methodology and assembly for the apparatus used to combine refrigerant vapor and airflow to get a desired concentration of refrigerant in the gas flow. The apparatus described in this section is close to the apparatus that is used to conduct the test for contamination effects as described by UL 60335-2-40. The UL 60335-2-40 does not specify how the apparatus should be designed or constructed. This means that there are many other options than the apparatus proposed in this section. The differences in the apparatus used for contamination effects is described later in Chapter 4. The design for this apparatus is a modification of the original apparatus design used by Wack [10].

To test the NDIR sensor, an apparatus had to be constructed that was capable of delivering an approximately known concentration of refrigerant vapor in air to the sensor. Figure 2.5 shows the test apparatus used by Wack [10]. Figure 2.6 shows the schematic of the slightly modified version of the test apparatus for the purpose of this paper. Two rotameters of the same size were mounted to a board. One of these rotameters was connected to the shop air provided, and the other

was connected to the refrigerant of interest. PVC flexible tubing was used to connect the rotameters to the sources of refrigerant and air. A pressure regulator and temperature probe were connected also using the flexible PVC tubing between the refrigerant source and the refrigerant rotameter. This allowed for the pressure of the flow to be adjusted before entering the rotameter, as well as for monitoring the temperature of the refrigerant supply. Also connected to the pressure regulator and thermometer probe was a needle valve. This needle valve was used to adjust the flow of the incoming refrigerant before it entered the rotameter. The pressure regulator, thermometer probe, and needle valve were all mounted to the same board as the rotameter. The rotameter was calibrated so that the height of a plastic tracking ball inside the rotameter corresponded to the volumetric flow rate.

For the air source, PVC flexible tubing was used to connect the rotameter for air to a shop air supply. The airflow also had a pressure gauge and a needle valve to control the flow between the air source and the rotameter. Both the pressure gauge and needle valve were also mounted to the board. PVC flexible tubing was used to connect the outlet of both rotameters to a tee connection where the gas flows mixed. From the teen connection, more PVC flexible tubing was used to extend the outlet of the gas flow to the test chamber where the gasses could mix and reach equilibrium. After the conclusion of the test, the test chamber would be manually emptied under a fume hood for safe ventilation.

The test chambers used for this research were 13 gallon polyethylene bags. The outlet of the gas flow was put into the trash bag and held closed by hand until the bag was filled with gas. Once the bag was filled with gas, the bag would be opened briefly allowing enough time for all the sensors to be tested to be placed into the bag. The bag was held closed by hand for the duration of the test.

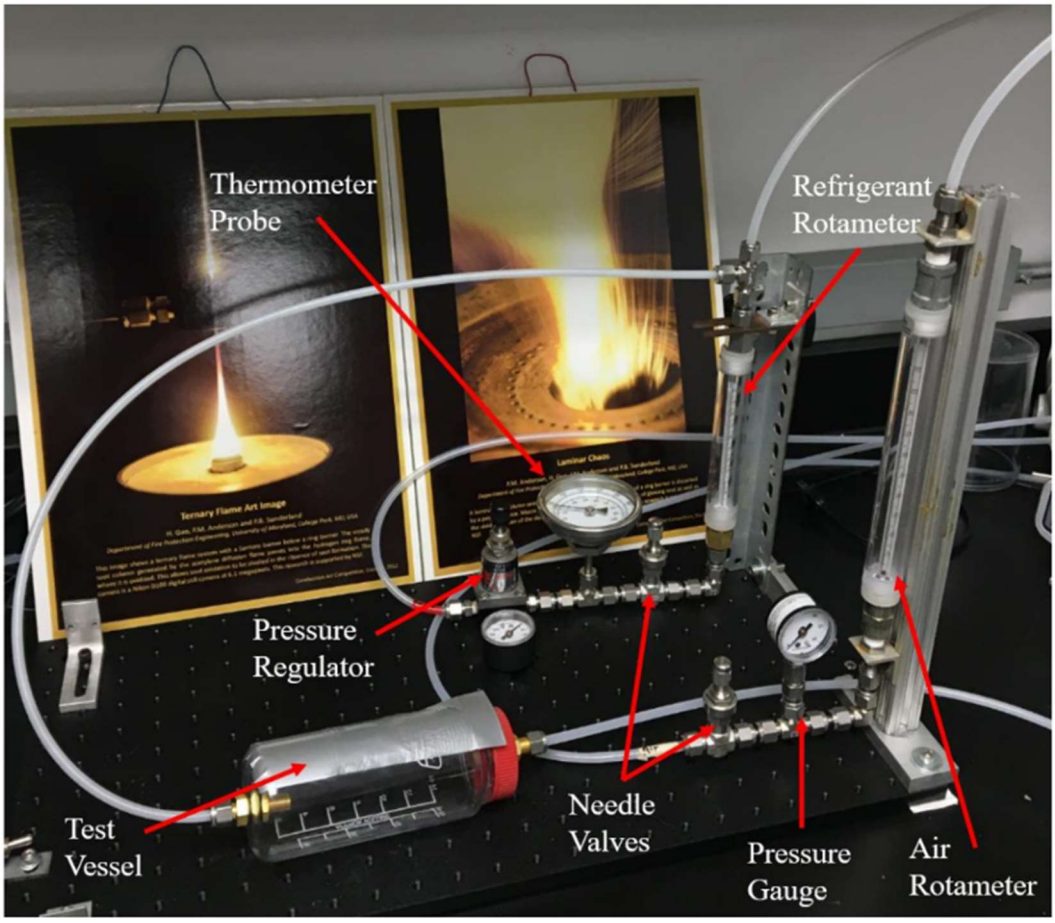

Figure 2.5 Test apparatus constructed by Wack [10]. Reproduced from [10]

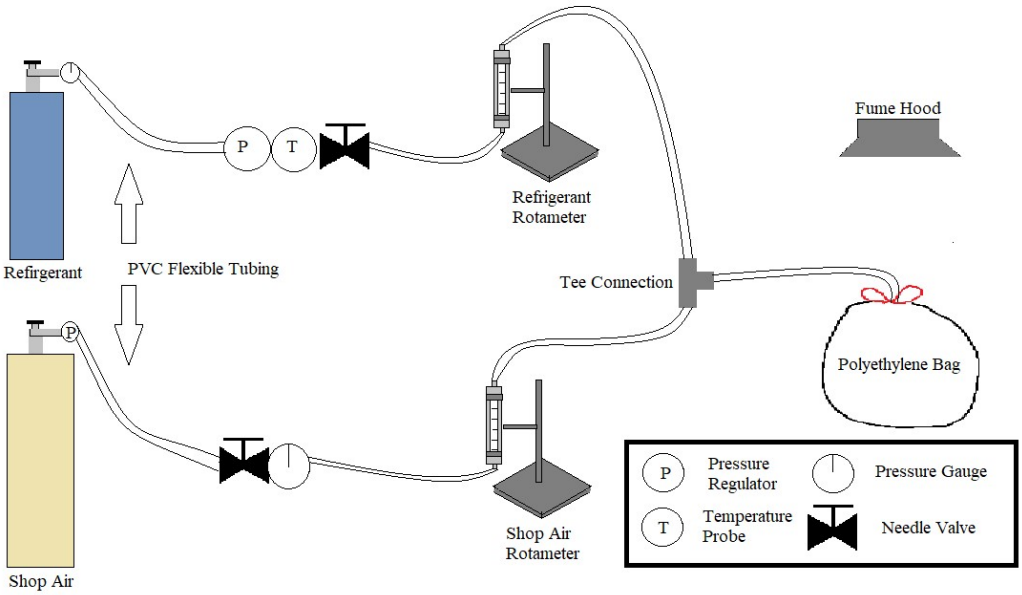

Figure 2.6 Modified test apparatus.

2.4 Soap Bubble Calibration

To accurately measure the flow rates of the gasses that were being mixed, it was necessary to know how much gas was flowing through each rotameter. The rotameters each had a tracking ball that would be pushed up the rotameter when gas flowed through it. This tracking ball would reach a steady state height which would correspond to the amount of gas flowing through the rotameter. This tracking ball height correlation is unique to the gas flowing through the rotameter. Because of this, a method for calibrating the rotameters to each gas flowing through the rotameters was needed. The method proposed in this paper used soap bubbles to measure the flow rates. This method was deemed sufficiently accurate and was used to calibrate the rotameters to any of the gasses required for testing.

Soap bubble flow meters are long glass tubes that have tick marks that indicate the amount of volume is between the tick mark and the bottom of the flow meter. Soap bubble flow meters have a wide range of available volumes, but for these tests a soap bubble flow meter of 100 mL with tick marks indicating every 20 mL of volume was used. The soap bubble flow meters have a gas inlet near the bottom of the long glass tube. The top of the tubes typically were open or have a small outlet for the gas to escape. At the bottom of the glass tube, just below the gas inlet, is a rubber pipet that contains a soap solution. When gas flows through the inlet, the rubber pipet is squeezed to form a soap bubble. The incoming gas pushes the soap bubble up the flow meter. The volumetric flow rate is determined by measuring how much volume the soap bubble is pushed through against the time it took for the soap bubble to be pushed through that volume. Figure 2.7 shows the soap bubble flowmeter that was used to calibrate the gasses used.

Figure 2.7 Image of soap bubble flow meter used for calibration.

To use this method to calibrate the rotameters, PVC flexible tubing was used to connect the outlets of the rotameters to the inlet of the soap bubble flow meters. Starting with the shop air, the shop air was allowed to flow into the test apparatus, making sure the needle valve was closed so that no air got into the rotameter. Next, the needle valve was adjusted so that the tracking ball was pushed to a height of around 20 on the rotameter. The tracking ball height was allowed to stabilize, and the height of the tracking ball was recorded using the bottom of the tracking ball as the reference point. Then the rubber pipet filled with the soap solution was squeezed gently until a soap bubble was formed. The soap bubble would be pushed up the flowmeter by the incoming gas from the rotameter. When the soap bubble passed the 0 mL tick mark, a timer was started. After the soap bubble had passed the 20 mL tick mark, the timer would be stopped and the time

would be recorded. This process was repeated three times at the same tracking ball height. The volumetric flow rate for the corresponding tracking ball height was the average of these three measurements. This process was repeated at an in interval of roughly 20 ticks on the rotameter. This process gave 5 calibrated volumetric flow rates. This was repeated for each gas that required a rotameter flow rate calibration.

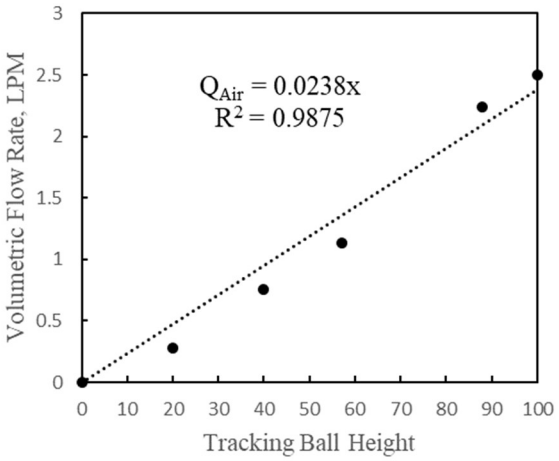

(a) Shop air flow calibration

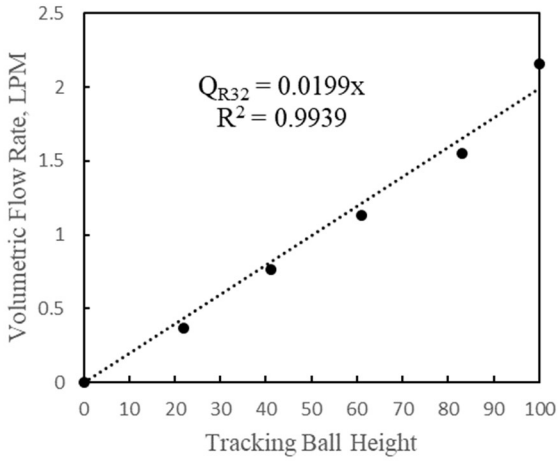

(b) R-32 flow calibration

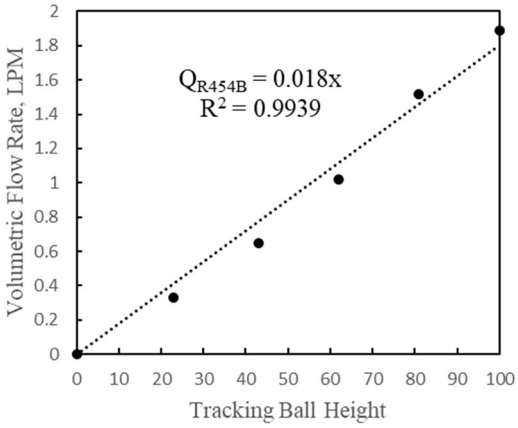

(c) R-454B flow calibration

Figure 2.8 Calibrated flow rates as a function of tracking ball height.

The raw measurements in s/20 mL were converted to L/min. These 5 calibrated flow rates were plotted against their corresponding tracking ball height. A trend line was used to fit the flow rates into a function of tracking ball height. Figure 2.8 (a) shows the relationship between tracking ball height, x, and shop air flow rate, Q_{Air}. Figure 2.8 (b) shows the relationship for R-32 flow rate, Q_{R32}, and Figure 2.8 (c) shows the relationship for R-454B flow rate, Q_{R454B}. All three of the gasses used showed a linear relationship between gas flow rate and tracking ball height. Now that the flow rates of the gasses can be reasonably estimated using the linear trend line relationships, the concentration of the refrigerant can be determined. The percent of the LFL for the refrigerants can be described by

$$LFL\% = (Q_r / [Q_r + Q_{Air}]) / LFL. \tag{2.1}$$

In equation 2.1, $LFL\%$ is the desired percentage of the refrigerant in use. Q_r is the volumetric flow rate of the refrigerant. LFL is the LFL by volume percent of the refrigerant in use. The LFLs for R-32 and R-454B are 14% [24] and 11.25% [25] respectively. The soap bubble methodology in conjunction with equation 2.1 allows for a range of LFL percentages to be used for testing.

Chapter 3: Sensor Response to Refrigerants

3.1 Bag Plunge Tests

Part of understanding a sensor's response to refrigerant concentrations is to measure how long it takes for the sensor to detect that there was a change in concentration from when the sensor was initially exposed. This time is called the sensor's response time. The response time not only includes the amount of time it takes for the sensor to initially react to the presence of refrigerant vapors, but the amount of time it takes for the sensor to report that a concentration threshold has been crossed. Annex LL, Section 3 of UL 60335-2-40 standard was recently updated to now state that this response time shall not be over 10 seconds after the initial exposure. The recent updates also state that this concentration threshold shall be 25% of the refrigerants LFL. The response time shall be measured by exposing the detection system to 100% of the refrigerant LFL and measuring how long it takes the system to cross the 25% LFL threshold [7]. To perform this test, the 25% LFL set point from the NDIR sensor must be measured. This response time was measured through bag plunge tests.

To perform a bag plunge test, the supply for both the refrigerant and shop air are allowed to flow to the rotameters. Using the needle valve and equation 2.1, the rotameters are adjusted to create a flow of the desired percentage refrigerant LFL. The gas mixture was allowed to flow into the polyethylene bag until the bag was full and started to push outwards. When the polyethylene bag was full, the needle valves were closed to stop the flow of gas. Just before the NDIR sensor was exposed to the gas mixture, the time of the beginning of the test was recorded down to the second. After the time was recorded, ten seconds were allowed to pass to show the NDIR sensor's

ambient response. The polyethylene bag was then quickly opened, and the NDIR sensor was plunged into the center of the bag. The polyethylene bag was then quickly closed. The NDIR sensor was kept in the bag mixture for 120 seconds, or long enough for a steady state output to be achieved by the NDIR sensor. Next the NDIR sensor was taken out of the polyethylene bag and allowed to recover in ambient air. The time that the NDIR sensor was taken out of the polyethylene bag was recorded.

The UL 60335-2-40 only requires that the sensor's 25% LFL set point be measured to characterize the sensor response time. To better understand the NDIR sensor response varying concentrations of refrigerant, steady state set points were measured using the bag plunge test at 25% LFL, 50% LFL, 75% LFL, and 100% LFL. Starting at 25% LFL the NDIR sensor would undergo the bag plunge test. The NDIR sensor was allowed to recover in ambient air for a full hour before doing another bag plunge test. The concentration would be increased to the next highest testing point and the bag plunge test would be repeated until the 100% LFL bag plunge test was concluded. Primarily the NDIR sensor is calibrated to measure gas concentrations for refrigerants including R-1234yf, R-1234ze, and R-32 [22]. Refrigerants R-32 and R-454B were chosen to test with the NDIR sensor to observe the sensor behavior of a factory calibrated refrigerant and a refrigerant that wasn’t factory calibrated.

Figure 3.1 shows the sensor output for the bag plunge tests at 25%, 50%, 75% and 100% of the LFL for R-32 and R-454B. The output of the NDIR sensor is gas concentration by volume percentage. In all the bag plunge tests, it took the NDIR sensor about 30 seconds to reach its peak output. For the 25%, 50%, and 75% LFL bag plunge tests, the output was stable as soon as the peak output was recorded. Only in the 100% LFL bag plunge test, seen in Figure 3.1d, did the output take additional time to stabilize. In this bag plunge test, the NDIR sensor reaches a peak

concentration in 30 seconds of about 8.82% and 7.55% for R-454B and R-32 respectively. Over the next 40 seconds, the output gradually declines until the 70 second mark where the output stabilizes. As the percentage of the refrigerant LFL increased, so did the output. The stabilized output for both R-32 and R-454B were within about 1% of each other. This indicates that the sensor can perform relatively accurately on refrigerants other than the ones specifically listed that are measured. Also, as the percentage of the LFL increases, so does the steepness of the output curve. Since the outputs all reached their peak around 30 seconds, the results indicate the NDIR sensor was able to respond to higher concentrations of refrigerant within the same amount of time as it takes to respond to lower concentrations of refrigerant. For all the bag plunge tests, the output reports slightly higher concentrations of refrigerant for the R-454B trials than the R-32 trials. The output curve for R-454B is also slightly higher than the output curve for R-32 indicating that the NDIR sensor responded slightly faster to R-454B than to R-32.

The only sensor that reacted to the ambient lab air or the shop air that was used to create the gas mixtures was the SS sensor with an ambient output of 2.2% LFL. R-454B has a lower LFL than R-32 with a value of 11.25% versus 14% [24-25]. This means that at all these percentages of the LFL, less R-454B is needed in the mixture to obtain the desired LFL percentage than R-32. However, even at a smaller concentration of gas, R-454B had a slightly higher steady state output than R-32 in each of the tested percentages of the LFL. The one fact that may be causing this observation is that the NDIR sensor is not calibrated to respond to R-454B while it is calibrated to respond to R-32. While the NDIR sensor does a good job of producing consistent results for both types of refrigerants, an unknown bias may be included in the NDIR sensor output for R-454B. Another anomaly that was observed is that the NDIR sensor outputs were slightly lower than expected. At 100% of the LFL, outputs of 11.25% and 14% for R-454B and R-32. were expected.

These procedures were repeated on the MPS sensor, thermal conductivity sensor, and the SS sensor to compare to the NDIR sensor output. These results are summarized in Figures 3.1 – 3.4 and Tables 3.1. As seen in both Figure 3.1 and Table 3.1, much smaller output values compared to actual concentration were observed. Since the NDIR sensor is still in the development phase, observations like this will help future calibrations.

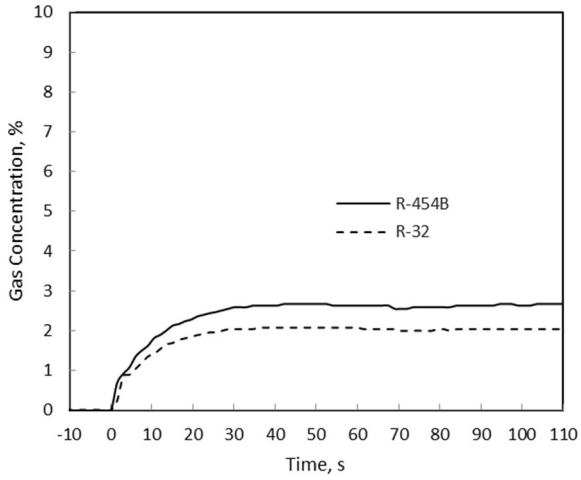

(a) 25% LFL

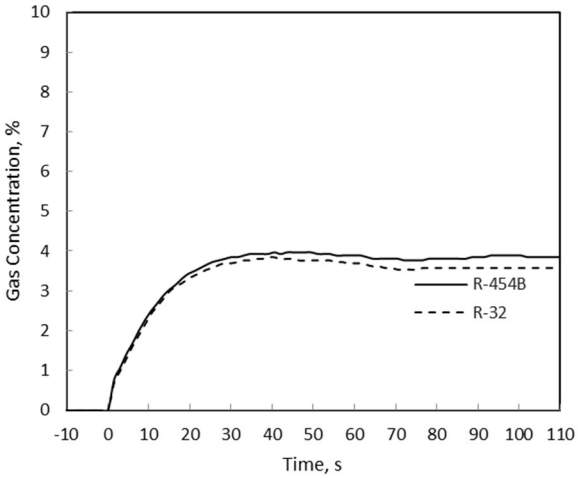

(b) 50% LFL

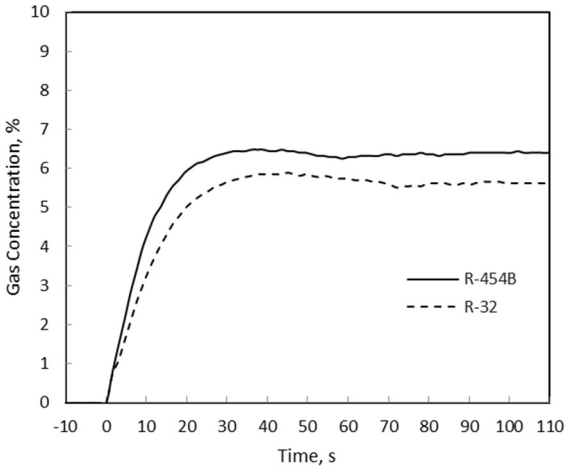

(c) 75% LFL

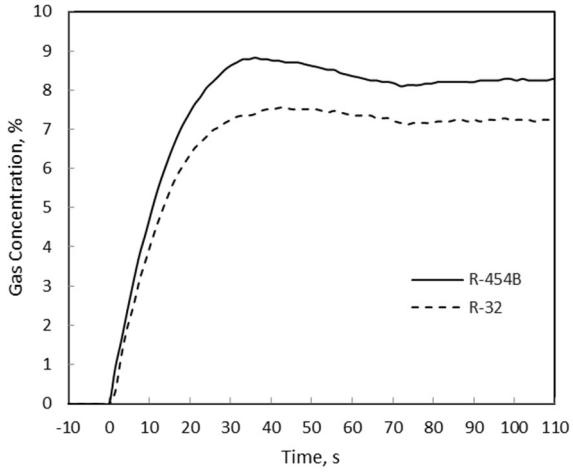

(d) 100% LFL

Figure 3.1. NDIR sensor response to varying concentrations of refrigerant. (a) 25% LFL, (b) 50% LFL, (c) 75% LFL, and (d) 100% LFL.

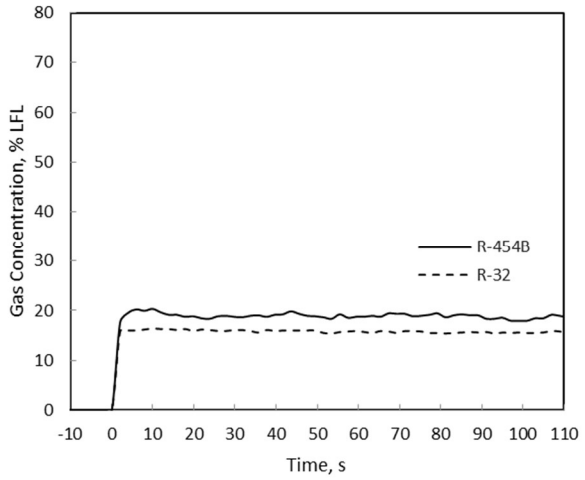

(a) 25% LFL

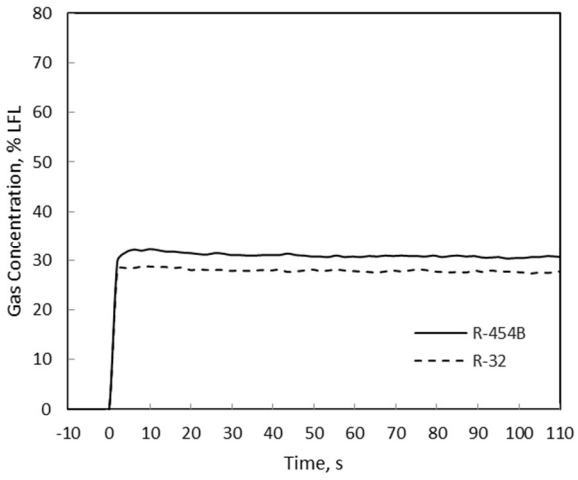

(b) 50% LFL

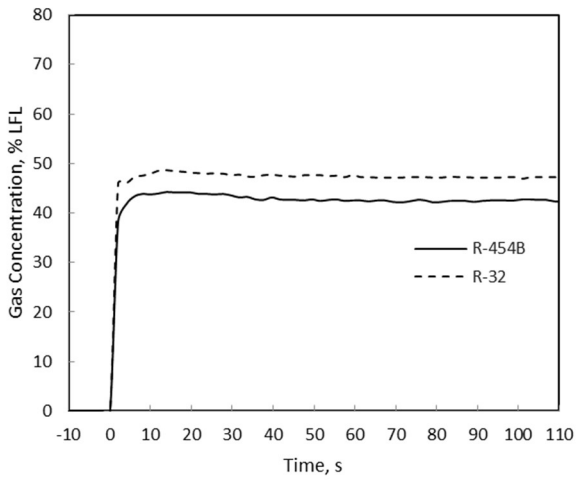

(c) 75% LFL

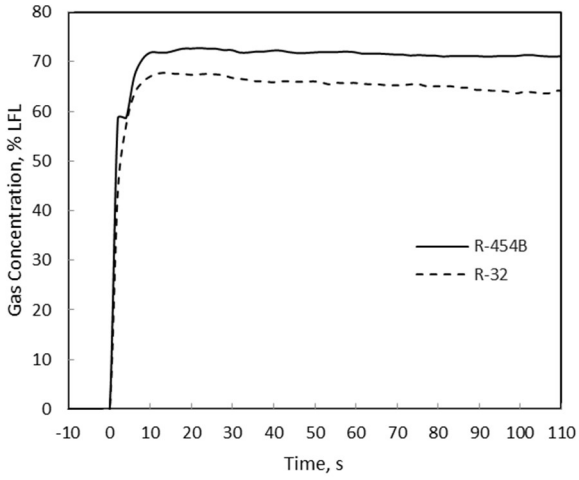

(d) 100% LFL

Figure 3.2. MPS sensor response to varying concentrations of refrigerant. (a) 25% LFL, (b) 50% LFL, (c) 75% LFL, and (d) 100% LFL.

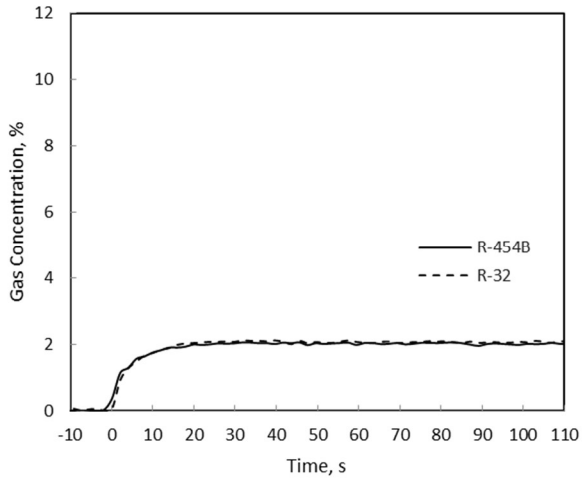

(a) 25% LFL

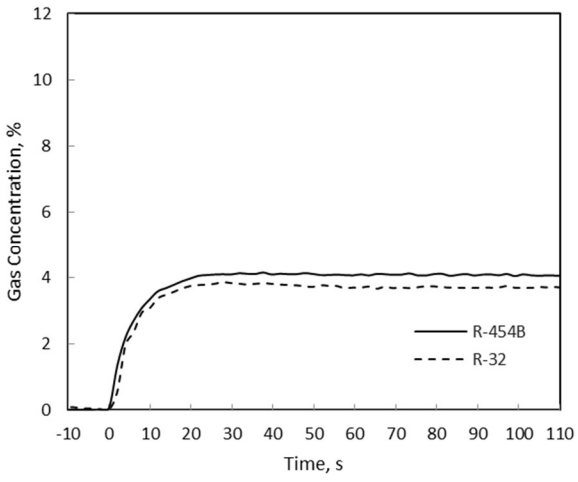

(b) 50% LFL

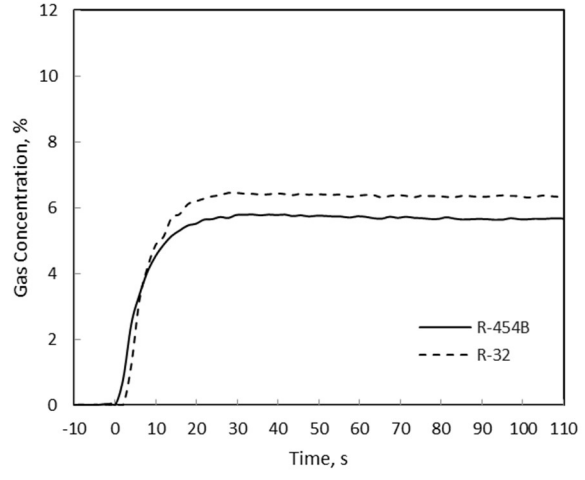

(c) 75% LFL

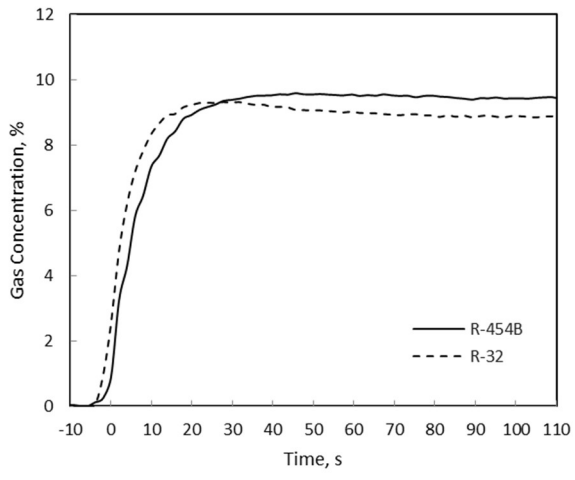

(d) 100% LFL

Figure 3.3. Thermal conductivity sensor response to varying concentrations of refrigerant. (a) 25% LFL, (b) 50% LFL, (c) 75% LFL, and (d) 100% LFL.

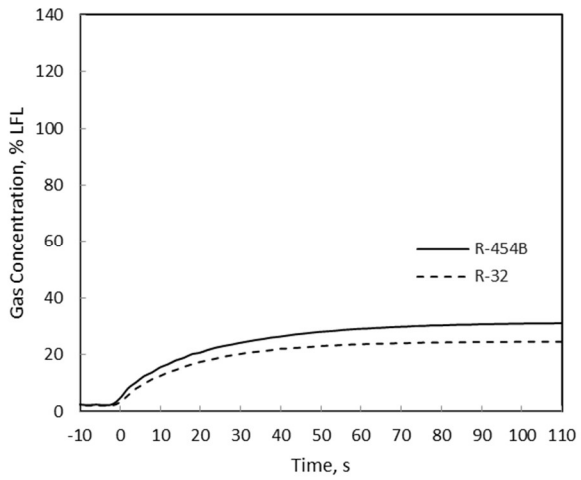

(a) 25% LFL

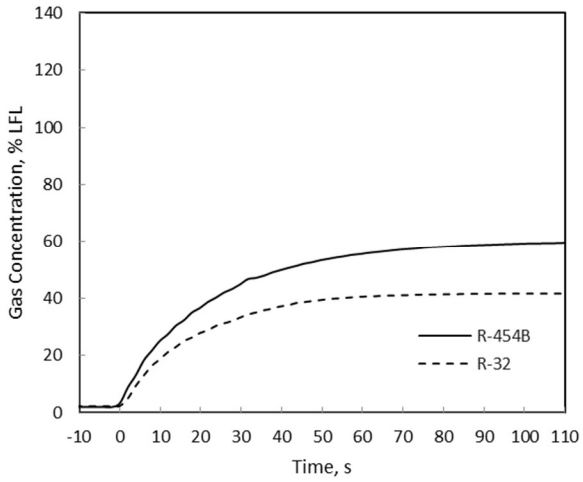

(b) 50% LFL

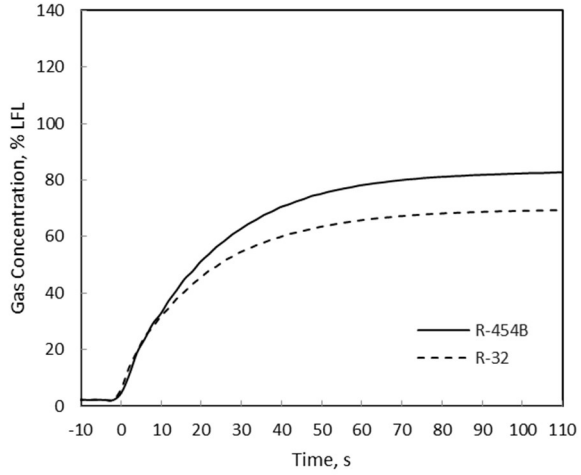

(c) 75% LFL

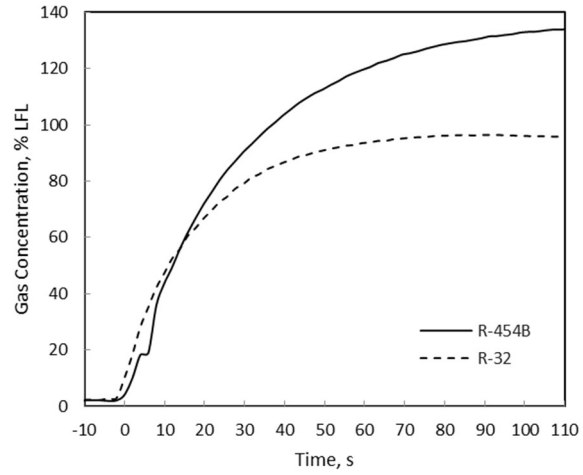

(d) 100% LFL

Figure 3.4. SS sensor response to varying concentrations of refrigerant. (a) 25% LFL, (b) 50% LFL, (c) 75% LFL, and (d) 100% LFL.

Table 3.1. 25% LFL steady state output for each sensor output.

Refrigerant	NDIR	SS	MPS	TC
R-454B	2.69	31.3	15.7	2.06
R-32	2.08	14.7	15.5	2.05

Table 3.1 summarizes the bag plunge tests. It shows the steady state outputs of the sensors when they were exposed to 25% of the LFL of the refrigerant. This steady state output value is the alarm threshold. Figure 3.1 shows the NDIR sensor response to 25, 50, 75, and 100% LFL for R-454B and R-32. The sensor tended to have a higher output for R-454B than for R-32. The NDIR sensor also responded in a similar amount of time for both refrigerants. At 25% LFL the NDIR sensor had a steady state output of 2.69% and 2.08% for R-454B and R-32. The NDIR sensor had a 100% LFL steady state output of 8.39% and 7.05% for R-454B and R-32 respectively. This shows that the safety factor of 4 that the UL 60335-2-40 standard is trying to achieve is not quite reached from these bag plunge tests. Instead, the results indicate a safety factor between 3 and 3.5, even at the peak sensor outputs for 100% LFL.

Figure 3.2 shows the MPS sensor response to 25, 50, 75, and 100% LFL for R-454B and R-32. The MPS sensor responded instantly to both R-32 and R-454B. The MPS sensor also tended to have a higher output for R-454B. The MPS sensor had a 25% LFL steady state output of 15.7% LFL for R-454B and 15.5% LFL for R-32. When exposed to 100% LFL, the steady state values were 70.7 and 64.5 for R-454B and R-32. The MPS sensor does achieve a safety factor of 4 or better for each refrigerant.

Figure 3.3 shows the thermal conductivity sensor response to 25, 50, 75, and 100% LFL for R-454B and R-32. The showed approximately the same outputs for both R-32 and R-454B with the same rate of change. At 25% LFL exposure, the steady state values were 2.06% concentration and 2.05% concentration for R-454B and R-32 respectively. At 100% LFL exposure they were 9.46% and 8.74%. This means this sensor would meet the safety factor of 4.

Figure 3.4 shows the SS sensor response to 25, 50, 75, and 100% LFL for R-454B and R-32. This sensor had a much higher output for R-454B than for R-32 and took longer to reach steady

state in the 100% exposure test. For 25% LFL exposure they were 31.3% and 14.7% LFL for R-454B and R-32. At 100% they were 137.9% LFL and 95.8% LFL. This sensor also meets the safety factor of 4.

Figure 3.5 shows the linear relationships of the steady state output for the NDIR, thermal conductivity, SS, and MPS sensor output and the actual percentage of the LFL for R-454B and R-32. As expected, when the concentration of the refrigerant increased linearly, the sensor's output also increased linearly for both R-454B and R-32. The NDIR sensor had the best relationships for both R-454B and R-32 with R^2 values of 0.9968 and 9989 respectively. The thermal conductivity sensor had the worst relationship for R-454B with a R^2 value of 0.9895, and the SS sensor had the worst relationship for R-32 with a R^2 value of 0.9932. However, all the sensors still had strong linear relationships when comparing output vs actual concentration. This means that even though the sensor output may not be accurate, it is still responding to the changes in concentration proportionally.

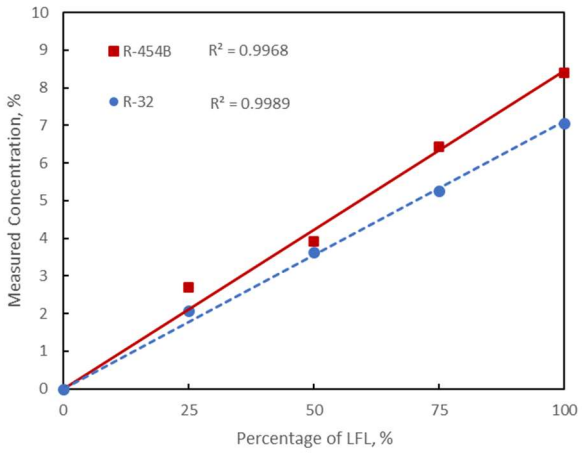

(a) NDIR sensor

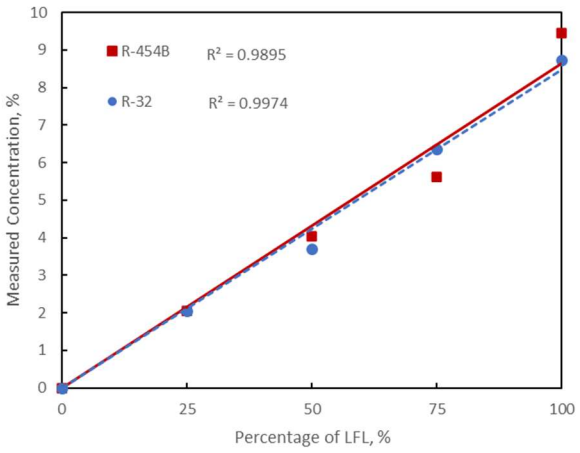

(b) Thermal conductivity sensor

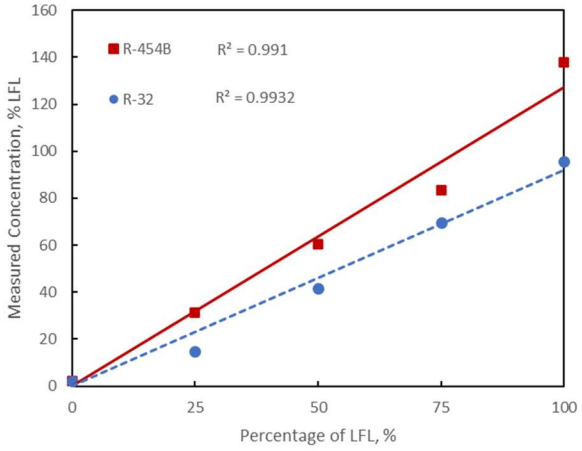

(c) SS sensor

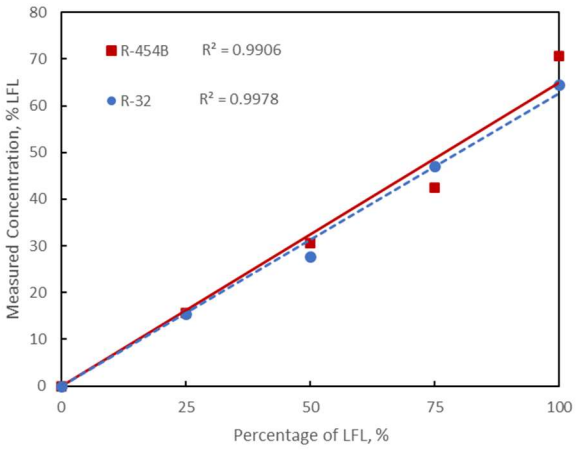

(d) MPS sensor

Figure 3.5. Linearity of the (a) NDIR, (b) thermal conductivity, (c) SS, and (d) MPS sensor's response to the varying percentages of the LFL.

3.2 Sensor Response Time Tests

The response time is measured by plunging the sensor into 100% of the LFL of a refrigerant and measuring how long it takes for the sensor to cross the 25% LFL steady state threshold from the moment the sensor was exposed to the refrigerant. The procedure is the same as the bag plunge

test except that only one plunge into 100% of the LFL is needed. Now that the sensor has a calibrated steady state response to 25% of the LFL via bag plunge tests, the response time test can be performed per the UL 60335-2-50 standard [7].

Figures 3.6 and 3.7 show the NDIR, thermal conductivity, SS, and MPS sensor response time test. The figures include the sensor response to 100% of the LFL with the 25%, 50%, and 75 % LFL thresholds are marked for reference. The sensor response in air before the plunge is shown as the sensor output before the time $t = 0$. After the plunge the sensor output begins to gradually increase from time $t = 0$ to $t = 20$. For the SS sensor, the time bounds were changed from -5 to 25 due to the sensor taking that long to respond. The sensor outputs were still increasing after 20 seconds, but it has already passed all the thresholds and has begun to level out.

Table 3.5 shows the response time for each of the trials. Since part of this study is better understanding the sensor's response to refrigerants, the response time for 50% and 75% of the LFL for each of the refrigerants was also included. For the response time that matters for the UL 60335-2-40 standard, the sensors were able to pass the 25% LFL threshold of 10 seconds. For R-454B, the MPS sensor had the fasted response time at 1 second, and the SS sensor had the slowest response time with 8 seconds. NDIR was middle of the pack with a response time of 5 seconds. For R-32, MPS again had the fastest response time at 1 second, and the SS sensor again had the slowest response time at 9 seconds. NDIR had a response time of 6 seconds. For the response time of the sensors at 50% of the LFL, only the SS sensor failed to have a response time under 10 seconds for both refrigerants. At 75%, both the NDIR and SS sensor did not have a response time under 10 seconds for both refrigerants. This means that the 25% LFL threshold could be potentially raised to 50% LFL for the NDIR sensor if nuisance alarms become a problem. As the concentrations increased, the response times stayed very similar to each other, being within 2

seconds of each other. For the NDIR, SS, and thermal conductivity sensor, the R-454B had the faster of the response times.

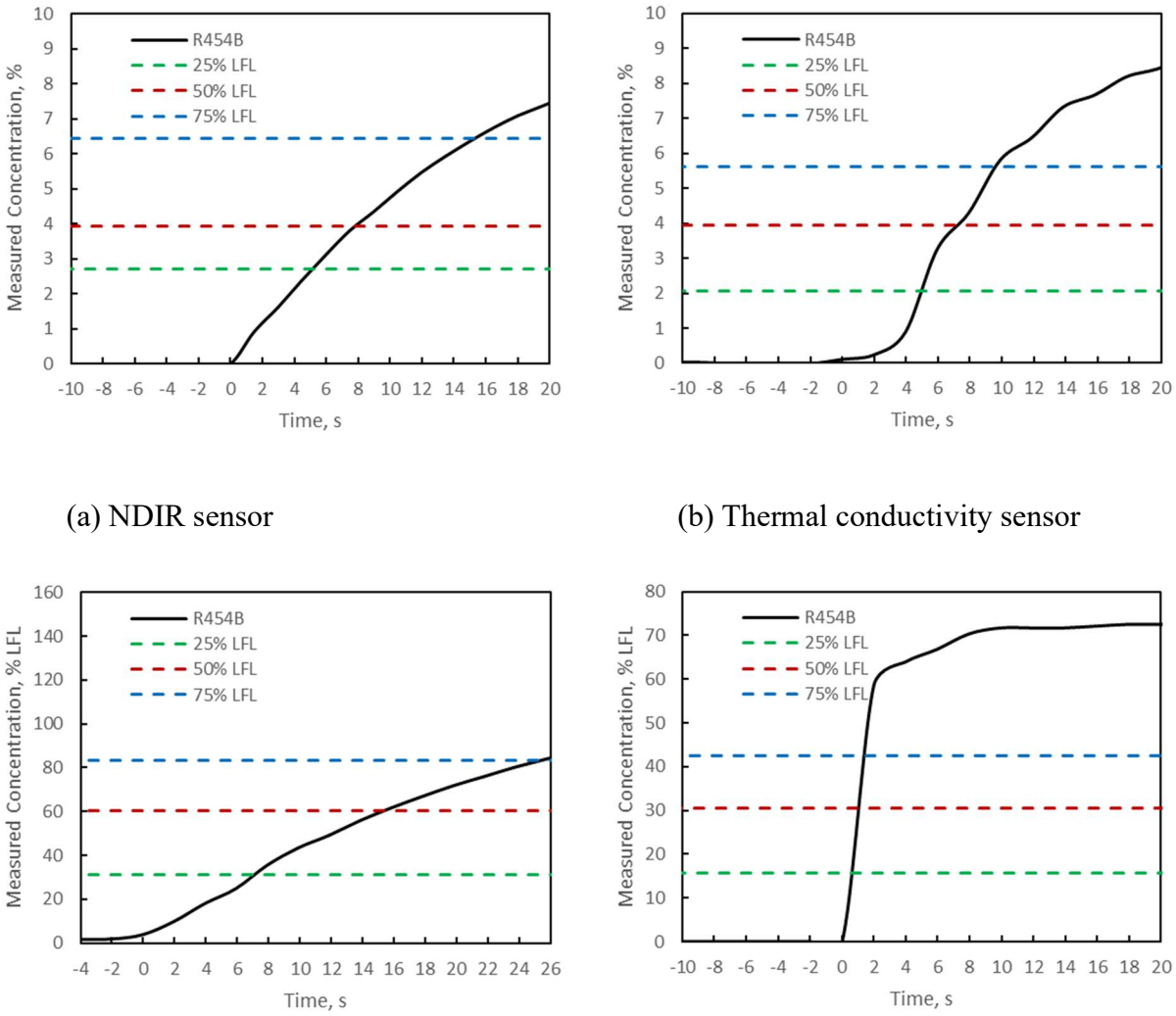

(a) NDIR sensor

(b) Thermal conductivity sensor

(c) SS sensor

(d) MPS sensor

Figure 3.6. Response time test for R-454B. (a) NDIR, (b) thermal conductivity, (c) SS, and (d) MPS.

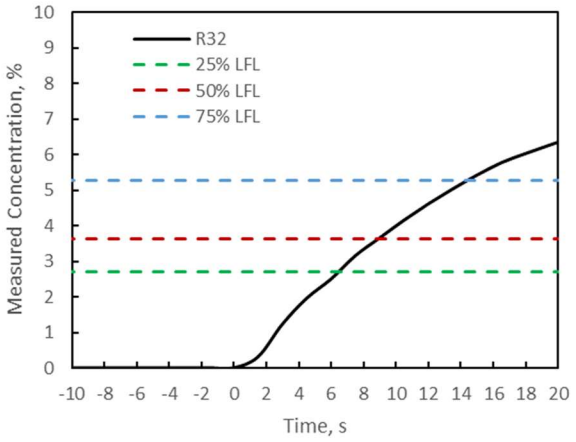

(a) NDIR sensor

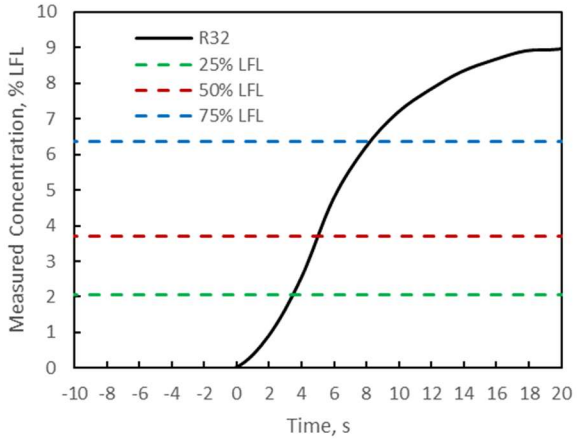

(b) Thermal conductivity sensor

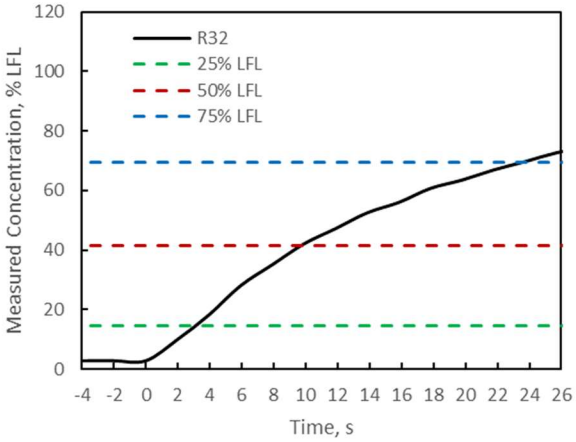

(c) SS sensor

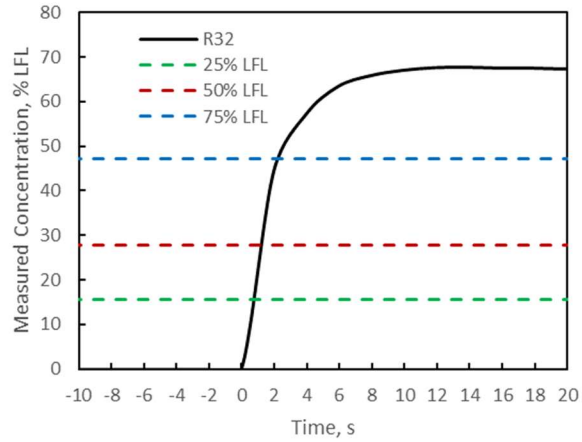

(d) MPS sensor

Figure 3.7. Response time test for R-32. (a) NDIR, (b) thermal conductivity, (c) SS, and (d) MPS.

Table 3.2. Response time in seconds for the sensors for varying concentrations of R-32.

Sensor	25% LFL	50% LFL	75% LFL
NDIR	4	10	14
MPS	1	1	1
SS	7	15	25
TC	3	5	8

Table 3.3 Response time in seconds for the sensors for varying concentrations of R-454B.

Sensor	25% LFL	50% LFL	75% LFL
NDIR	5	7.5	15
MPS	1	1	1
SS	8	16	25
TC	5	7	9

Chapter 4: Sensor Response to Contaminants

4.1 Contamination Test Procedure

One of the intended purposes for the sensors is to be installed and run in a residential application. This means that the sensors are subject to exposure to other chemicals that can be commonly found inside a residential building. These types of chemicals can come from beauty products, cleaning products, caulks, and paint products which all have the potential to mix with the ambient air, and therefore the sensor. It is important to know how these potential contaminants will affect the sensor. One possible outcome is that the sensor is poisoned. A poisoned sensor happens after being exposed to a contaminant, the sensor no longer produces a healthy/expected output curve. A poisoned sensor would have a different response time than the one previously characterized, and the sensor is no longer viable for refrigerant gas area monitoring. Another possible outcome is that when the sensor is exposed to a contaminant, it returns a false alarm. This means that when the sensor was exposed to the contaminant, the sensor started to output a signal. If the signal crosses the 25% LFL threshold previously described by the UL 60335-2-40 standard, the detection system would sound an alarm for the presence of an A2L refrigerant when there is none.

The UL 60335-2-40 standard in Annex LL contains a list of all the contaminants required to be used to test the sensor with [7]. This list of contaminants and the prescribed concentrations can be seen in Table 4.1. The list of contaminants includes chemicals that can be found in an everyday residential building, such as acetone in nail polish remover and isopropyl alcohol used in first aid application. The UL 60335-2-40 standard requires that the sensors not indicate the presence of a refrigerant concentration above the 25% LFL threshold [7].

All these sensors were able to be acquired for testing. Wack's [10] Table 4.1 shows the formula of each contaminant, the state that it was obtained in, and the concentration, X, the contaminants were received at. For the silicone contaminant, two chemicals were chosen to represent the contaminant. Decamethylcyclopentasiloxane was chosen due to it being a chemical that can be found in many popular household items such as toiletries and cosmetics. Octamethylcyclotetrasiloxane was chosen because of its presence in caulks which can off gas silicone particles into the air. In total, 13 contaminants were used to test the sensor response with. Four of the contaminants were ordered in a gaseous state, and the other seven were ordered as liquids. Only the chemicals *n*-Butane and Ammonia were pre-diluted with air upon ordering. The rest of the contaminants were pure in concentration.

Table 4.1. List of the procured contaminants and the concentration they were received at.

Chemical	Formula	MW_c, g/mol	Phase	X_{test}, ppm	X, %
Methane	CH_4	16.04	Gas	500	1
n-Butane	C_4H_{10}	58.12	Gas	300	0.009
Carbon Dioxide	CO_2	44.01	Gas	500	1
Ammonia	NH_3	17.03	Gas	200	0.0001
n-Heptane	C_7H_{16}	100.21	Liquid	200	1
Ethyl Acetate	$C_4H_8O_2$	88.11	Liquid	5000	1
Isopropyl Alcohol	C_3H_8O	60.1	Liquid	100	1
Ethanol	C_2H_5OH	46.07	Liquid	200	1
Toluene	C_7H_8	92.14	Liquid	200	1
Trichloroethane	$C_2H_3Cl_3$	133.40	Liquid	200	1
Acetone	C_3H_6O	58.05	Liquid	200	1
Decamethylcyclopentasiloxane	$C_{10}H_{30}O_5Si_5$	370.77	Liquid	100	1
Octamethylcyclotetrasiloxane	$C_8H_{24}O_4Si_4$	296.61	Liquid	100	1

The UL 60335-2-40 standard has a prescribed test procedure for exposing the sensors to the contaminants. Section 5 of Annex LL reads

"ensure that the chamber has been well ventilated with fresh air. Place the refrigerant sensor in operation inside the chamber and allow it to run for 15 ± 5 minutes. Close and seal the chamber to prevent air infiltration. Using a syringe or equivalent device, add the calculated amount of the first substance into the chamber at a rate and in a location such that it is well mixed with the air and does not cause localized high concentrations. Allow the refrigerant sensor to remain in the chamber for 2 hours. During this time the output shall not indicate the presence of refrigerant concentration above the (25% LFL equivalent response). Purge the chamber with clean air to remove all the test atmosphere. Maintain clean air in the chamber for a recovery time of 16 h or as specified by the manufacturer. In no case shall recovery time exceed 16 h. Reseal the chamber and repeat the test using another substance from [Table 4.1] until the refrigerant sensor has been exposed to all substances. It is not required that exposure to the substances be in any particular order" [7].

However, for these tests, the UL 60335-2-40 standard procedures were modified. Instead of a test chamber, the same polyethylene bags from the response time tests were used. The sensors were allowed to operate in air 15 minutes prior to exposure to the contaminants. Instead of using a syringe injection, the polyethylene bags were filled in the same manner they were filled in the response time tests. The flowmeters were used to adjust the concentrations of the contaminants and the gas flow was outlet into the polyethylene bag. The sensors were allowed to be inside the polyethylene bag for 2 hours. After the test, the test gas was expelled under a fume hood and the polyethylene bag was discarded. There was no need for purging since a new polyethylene bag would be used for every contaminant. The sensors were allowed to recover for 16 hours prior to the next contaminant exposure.

4.2 State of Health Tests

The UL 60335-2-40 standard defines a state of health test. Annex LL, Section 5 states that

"at the end of the [contaminant] test, the refrigerant sensor shall be tested in compliance with LL.3DV" [5].

The state of health test described in Section LL.3DV is the same response time test described in Chapter 3. The purpose of this state of health test is to check if the sensor no longer has the expected response time that it had from before the contamination. If the sensor does not respond as quickly as it did when it was healthy before exposure to a contaminant, the sensor is considered poisoned.

The state of health test was performed after exposing the sensor to each of the 13 contaminants prescribed in Table 4.1. The output from the state of health tests were compared to the output from Figure 3.1 as reference to a healthy sensor. The state of health test was conducted 16 hours after the conclusion of the final contaminant exposure to remain consistent with the procedures described in Section 4.1 of this Chapter.

4.3 Gas Contaminants

Four of the ordered contaminants were ordered in the gas phase. These contaminants were methane, *n*-butane, carbon dioxide and ammonia. *N*-butane and ammonia were ordered as a mixture of the gas and air. The apparatus depicted in Figure 2.6 was used for the gas contaminants, except the refrigerant supply line was instead connected to the contaminant supply. This required that the rotameters be calibrated to each of the gaseous contaminants. After the rotameters were calibrated, it was required to know how much air was necessary to dilute the contaminant concentration to the concentration specified in Table 4.1. To more easily solve this, the combined contaminant and air flow rate, Q_T, was set to 1 Lpm. This allowed for an easy solution to equation 4.1

$$Q_G = Q_T X_{test} / X, \tag{4.1}$$

where X_{test} is the prescribed concentration in parts per million (ppm) provided in Table 4.1, X is the original concentration fraction of the contaminant, and Q_G is the flow rate of the contaminant gas in Lpm. After having both Q_G and Q_T, the flow rate of air, Q_A, could be solved using equation 4.2

$$Q_A = Q_T - Q_G. \tag{4.2}$$

Table 4.2 shows all the calculated values for Q_T, Q_A, and Q_G. Methane and carbon dioxide required the most amount of air flow. This is due to both contaminants being ordered as a pure gas mixture. This means that the gas flow rates are very small. However, the gas flow rates can be increased to the rotameters capability by increasing Q_T. *N*-butane was available as a 0.9% butane-air mixture, meaning it required a 30:1 air flow to butane-air flow ratio to achieve the 300 ppm in Table 4.1. Ammonia was available at a 0.01% ammonia-air mixture. This means that the ammonia-air mixture did not have to be altered to achieve the 100 ppm requirement in Table 4.1

Table 4.2. Calculated contaminant and air flow rates in Lpm necessary for obtaining required contaminant concentrations.

	Q_T, Lpm	Q_G, Lpm	Q_A, Lpm
Methane	1	0.0005	0.9995
n-Butane	1	0.033	0.967
Carbon Dioxide	1	0.005	0.995
Ammonia	1	1	0

4.4 Liquid Contaminants

The other nine contaminants were obtained in their liquid states. In order to obtain the contaminant's vapors to mix into the gas flow, a filter flask assembly was used to bubble nitrogen through the liquid contaminant into the rotameter. Figure 4.2 shows a picture of the filter flask used. The assembly includes an inlet tube connected to a glass dispersion tube. This glass dispersion tube is fed through a rubber stopper on top of a 500 mL filtering flask to the bottom of the filtering flask. An outlet tube is located near the top of the filtering flask. Nitrogen was chosen as the gas to bubble through the contaminants to reduce potential hazards because some of the contaminants are flammable. Downstream from the filtering flask outlet, the vapors were mixed with air to dilute the gas mixture to the required concentration.

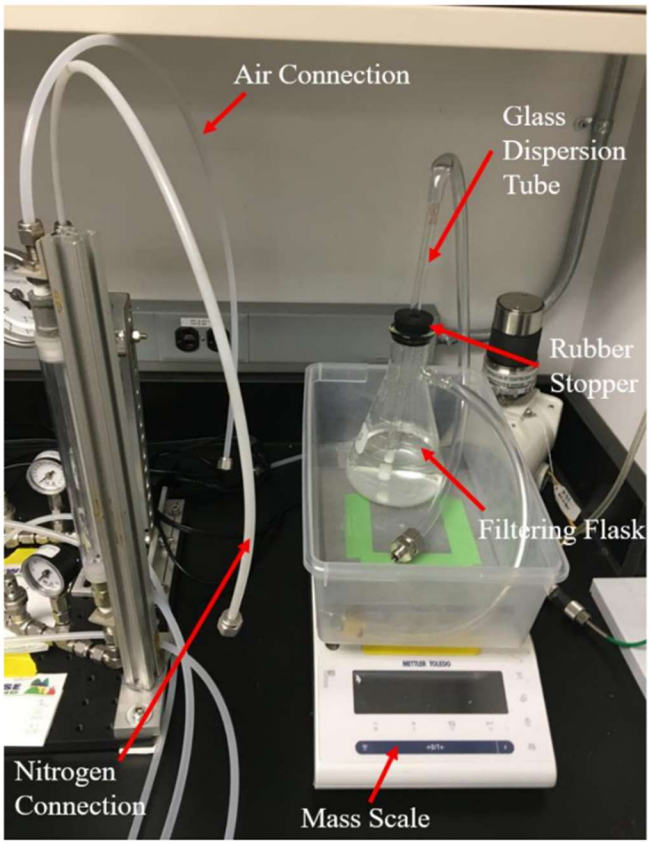

Figure 4.1. Filtering flask bubbling assembly. Reproduced from [10].

To determine the volumetric flow rate of the contaminant vapors, the mass loss rate of the liquid contaminant was calculated. This was done by measuring the initial mass of the filtering flask assembly, m_1, with a scale seen in Figure 4.1. Nitrogen was then allowed to bubble through the contaminant for 60 minutes. After this, the mass of the filtering flask assembly was measured again, m_2, to see how much of the vapor had flowed out of the assembly. This mass loss rate, $\dot{m}_v$, in g/min is described by

$$\dot{m}_v = (m_1 - m_2) / t, \tag{4.3}$$

where t is the test duration of 60 minutes. This mass loss rate can be used to determine the volumetric flow rate of the contaminant vapors, Q_v, with

$$Q_v = \dot{m}_v / \rho_c, \tag{4.4}$$

where ρ_c is the density of the contaminant. Using the ideal gas law, the density of the contaminant is calculated by

$$\rho_c = \rho MW_c \ / \ R_u T. \tag{4.5}$$

In equation 4.5, ρ is the atmospheric pressure, MW_c is the molecular weight of the contaminant found in Table 4.1, R_u is the universal gas constant, and T is the temperature during the time the bubbling took place. This temperature was measured using a thermometer probe and was observed

at 22°C. Lastly, the amount of air flow needed to dilute the contaminants to the specified concentrations in Figure 4.1 was calculated using

$$X_{Test} = Q_v / (Q_v + Q_{N2} + Q_A), \tag{4.6}$$

where Q_{N2} is the volumetric flow rate of nitrogen into the filtering flask assembly in Lpm.

Table 4.3 shows the calculated mass loss rate of the liquid contaminants and the volumetric flow rates of the contaminant vapors into the gas mix, the nitrogen into the filtering flask assembly, and the air into the gas mixture. The nitrogen volumetric flow rates used were based off Wack's [10] previous experiments bubbling nitrogen through the list of contaminants. These nitrogen flow rates were chosen because it was shown that they would require air flow rates within the tolerance of the rotameters used for experiments. The silicones required the most amount of nitrogen flow rate to produce a usable flow of contaminant vapors. This is likely due to these chemicals having low vapor pressures. Chemicals that have lower vapor pressure do not evaporate as easily then chemicals with higher vapor pressures. If the chemical does not evaporate quickly, more flow bubbling through the liquid is needed to induce evaporation. This can be seen again with ethyl acetate and acetone. These chemicals have higher vapor pressures and require the least amount of nitrogen bubbling to produce a useful contaminant vapor flow rate.

Table 4.4 shows the results from Wack's [10] bubbling experiments. In Table 4.4, $\dot{m}_{exp}$ is the same mass loss rate as calculated in Table 4.3. $Q_{vap,exp}$ and Q_{air} are the volumetric flow rates of the contaminant vapor and the air flow used to mix with the vapors. Most of the values for mass loss rate are comparable between the two experiments. Ethanol had the largest difference in measured mass loss rates with a difference of about 0.22 * 10^{-3} g/min. This difference meant that

about 0.6 Lpm more air flow was needed than what Wack [10] used to dilute ethanol in his experiments. Since the rest of the mass loss rate values were close to each other, the volumetric flow rates used were also relatively the same.

Table 4.3. Mass loss rate and volumetric flow rates for contaminant testing.

Chemical	$\dot{m}_v$, g/min * 10^{-3}	Q_{N2}, Lpm	Q_v, Lpm * 10^{-4}	Q_A, Lpm
n-Heptane	2.38	0.01	5.75	1.14
Ethyl Acetate	1.75	0.003	4.81	2.40
Isopropyl Alcohol	1.30	0.01	5.24	2.61
Ethanol	0.88	0.005	4.63	2.31
Toluene	1.70	0.01	4.46	2.22
Trichloroethane	1.36	0.035	2.47	1.20
Acetone	0.60	0.003	2.50	1.25
Decamethylcyclopentasiloxane	2.76	0.5	1.80	1.30
Octamethylcyclotetrasiloxane	2.46	0.1	2.01	1.91

Table 4.4. Results from Wack's bubbling experiments. Reproduced from [10].

	Q_{N_2}, Lpm	$\dot{m}_{calc}$, g/min	$\dot{m}_{exp}$, g/min	$Q_{vap,exp}$, Lpm	Q_{air}, Lpm
n-Heptane	0.01	2.29E-3	2.20E-3	5.32E-4	1.10
Ethyl acetate	0.003	1.38E-3	1.90E-3	5.22E-4	2.60
Isopropyl alcohol	0.01	1.29E-3	1.20E-3	4.84E-4	2.40
Ethanol	0.005	9.15E-4	6.60E-4	3.47E-4	1.70
Toluene	0.01	1.25E-3	1.60E-3	4.21E-4	2.10
Trichloroethane	0.035	5.36E-3	1.20E-3	2.18E-4	1.10
Acetone	0.003	2.61E-3	5.40E-4	2.25E-4	1.10
Decamethylcyclo-pentasiloxane	0.5	1.39E-3	2.83E-3	1.85E-4	1.40
Octamethylcyclo-tetrasiloxane	0.1	1.80E-3	2.40E-3	1.96E-4	1.90

4.5 Results

Figures 4.2 - 4.15 show the results from each contaminant as well as the response from different kinds of sensor technologies tested as well. Since the response time is based solely on the 25% LFL threshold as defined in the UL 60335-2-40 standard, the state of health tests will only include the 25% LFL threshold mark. Since the other sensing technologies were only tested in R-454B, the state of health test was also done in R-454B to draw better conclusions on sensor performance. The y axis of the MPS and SS sensor were changed to the same scale as the NDIR and TC sensor.

Methane

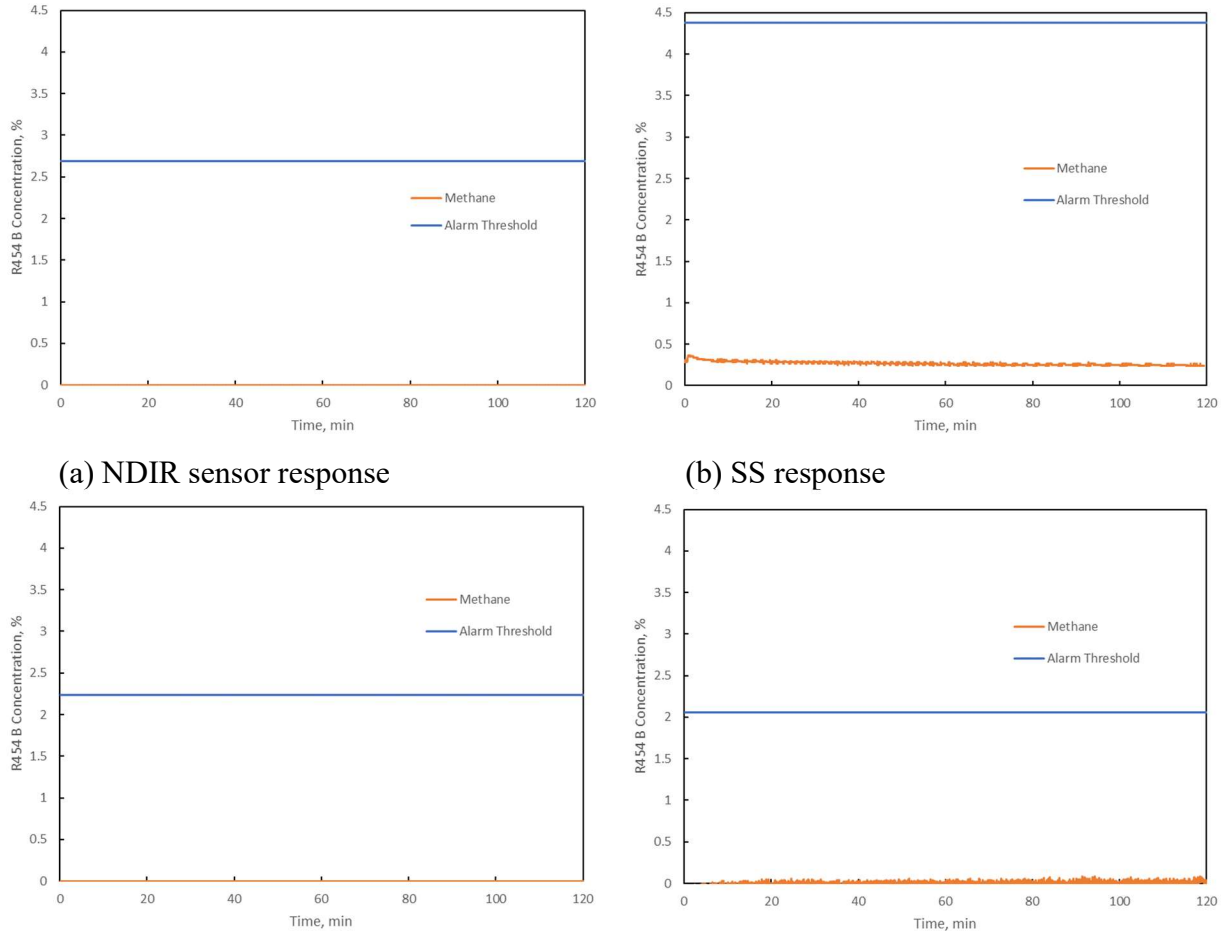

(a) NDIR sensor response

(b) SS response

(c) MPS sensor response

(d) Thermal conductivity sensor response

Figure 4.2. Results of methane contamination on (a) NDIR, (b) SS, (c) MPS, and (d) thermal conductivity sensor.

Figure 4.2 shows the sensor response to methane contamination. The NDIR sensor shows no change in output. This indicates that the UL standard 60335-2-40 specified concentration of methane does not have an effect on the NDIR sensor output. The thermal conductivity sensor and MPS sensor show no output change either. The SS sensor shows an output of 2% LFL, but the sensor was already showing an output of around 2% LFL before being exposed to methane.

n-Butane

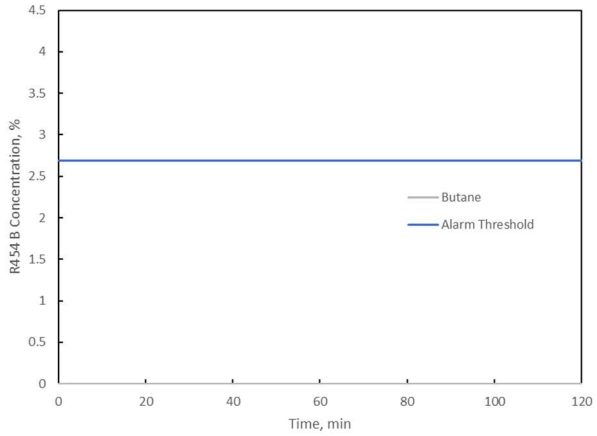

(a) NDIR sensor response

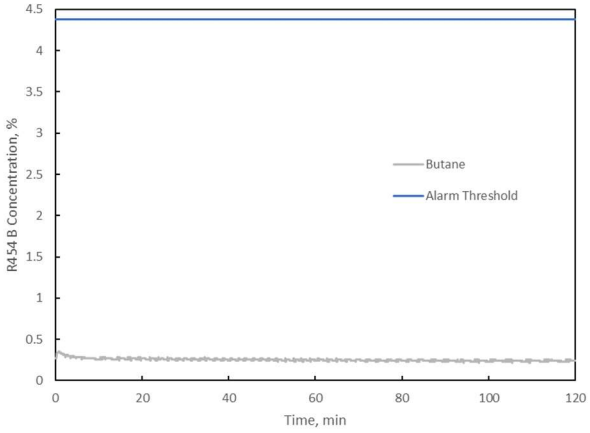

(b) SS response

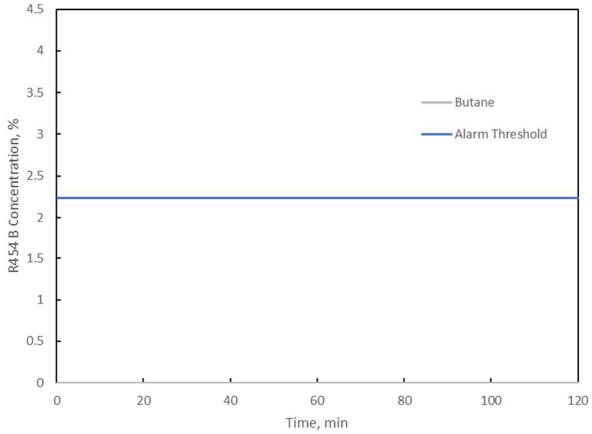

(c) MPS sensor response

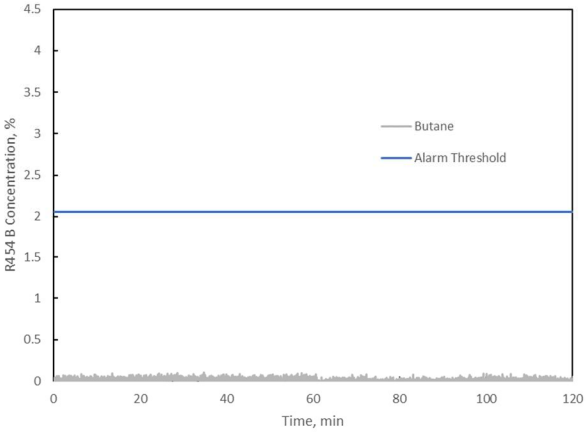

(d) Thermal conductivity sensor response

Figure 4.3. Results of *n*-butane contamination on (a) NDIR, (b) SS, (c) MPS, and (d) thermal conductivity sensor.

Figure 4.3 shows the sensor response to *n*-butane contamination. Similar to methane, the NDIR sensor shows no response to the contaminating chemical. This indicates that the UL standard 60335-2-40 specified concentration of *n*-butane does not have an effect on the NDIR sensor output. The SS, MPS, and thermal conductivity sensors also show no change in their baseline output.

n-Heptane

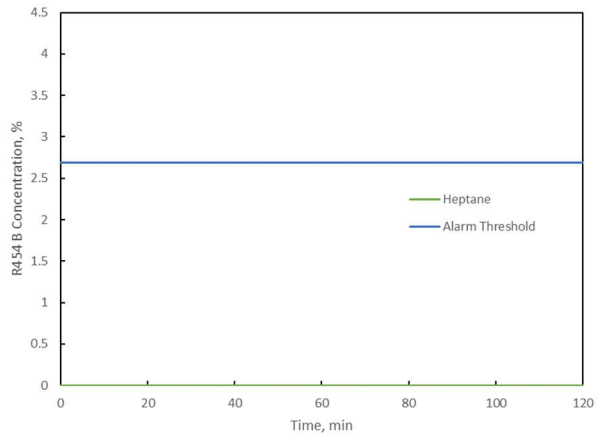

(a) NDIR sensor response

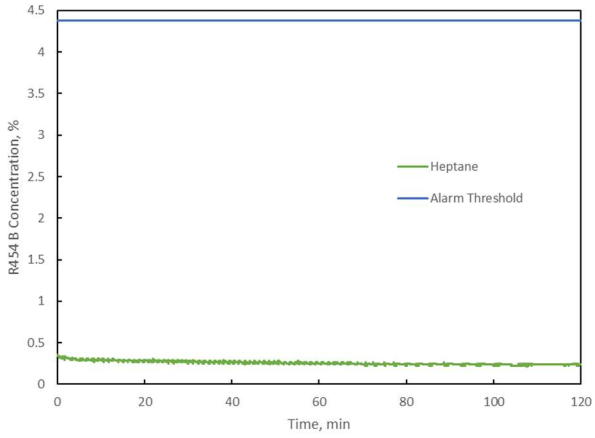

(b) SS response

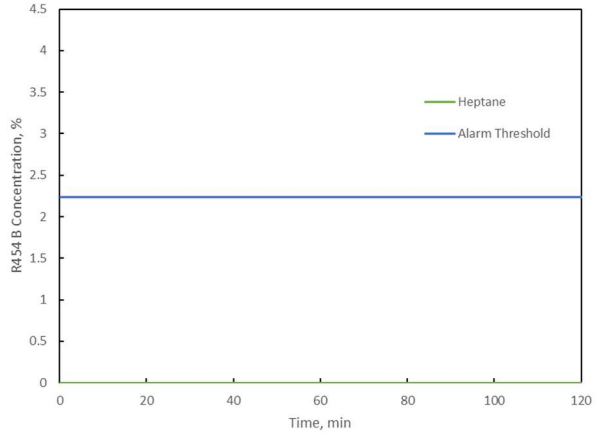

(c) MPS sensor response

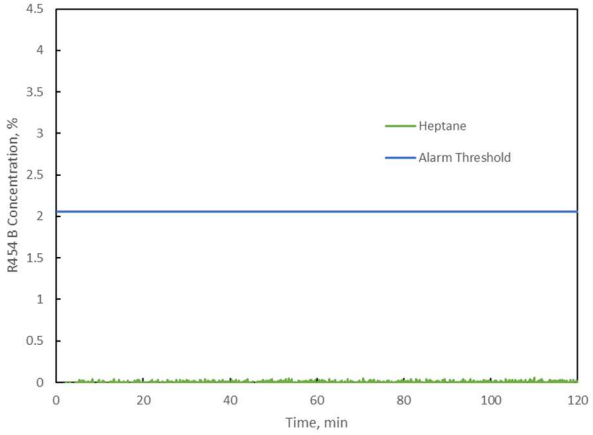

(d) Thermal conductivity sensor response

Figure 4.4. Results of *n*-heptane contamination on (a) NDIR, (b) SS, (c) MPS, and (d) thermal conductivity sensor.

Figure 4.4 shows the sensor response to *n*-heptane contamination. The NDIR sensor shows no response to the contaminating chemical. This indicates that the UL standard 60335-2-40 specified concentration of *n*-heptane does not have an effect on the NDIR sensor output. The SS, MPS, and thermal conductivity sensors also show no change in their baseline output.

Ethyl Acetate

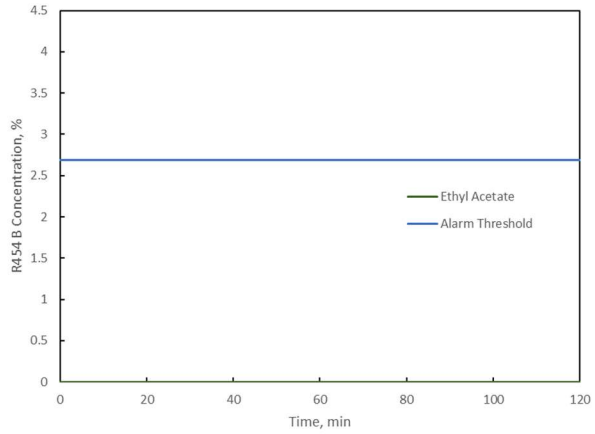

(a) NDIR sensor response

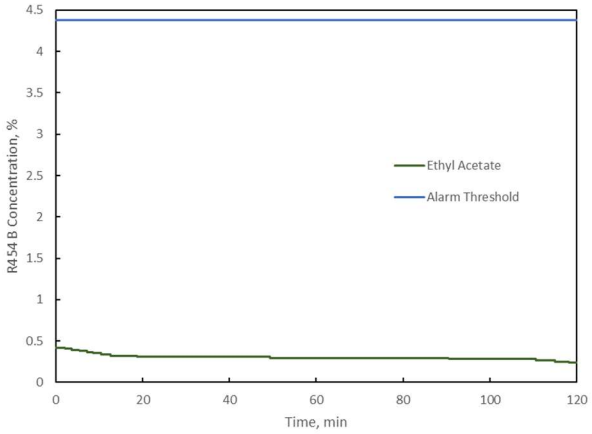

(b) SS response

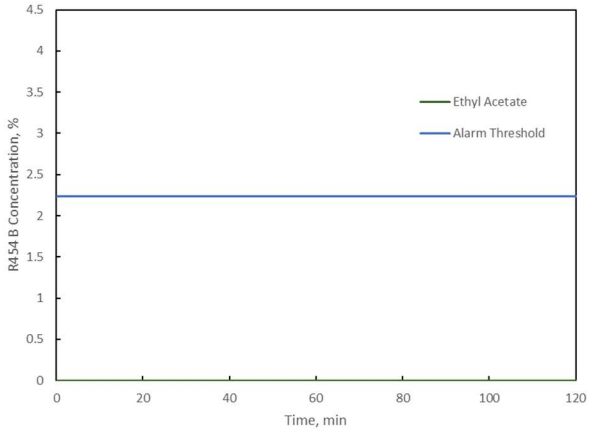

(c) MPS sensor response

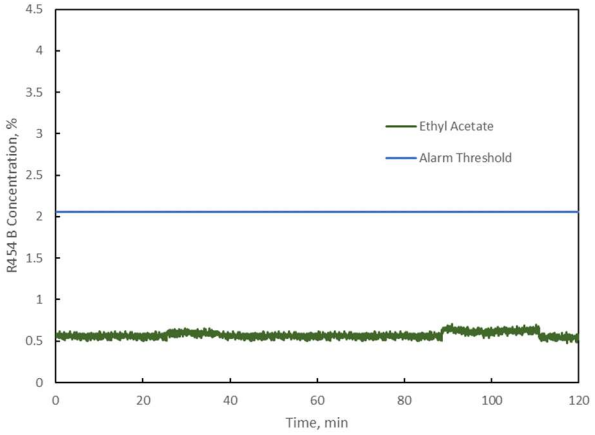

(d) Thermal conductivity sensor response

Figure 4.5. Results of ethyl acetate contamination on (a) NDIR, (b) SS, (c) MPS, and (d) thermal conductivity sensor.

Figure 4.5 shows the sensor response to ethyl acetate contamination. The NDIR sensor shows no response to the contaminating chemical. This indicates that the UL standard 60335-2-40 specified concentration of ethyl acetate does not influence the NDIR sensor output. The SS and MPS sensors do not show a change in output. The thermal conductivity sensor showed an increase in output from 0% R-454B concentration to 0.6% R-454B concentration. This increase is not close to the 25% LFL threshold of 2.06% for the thermal conductivity sensor.

Isopropyl Alcohol

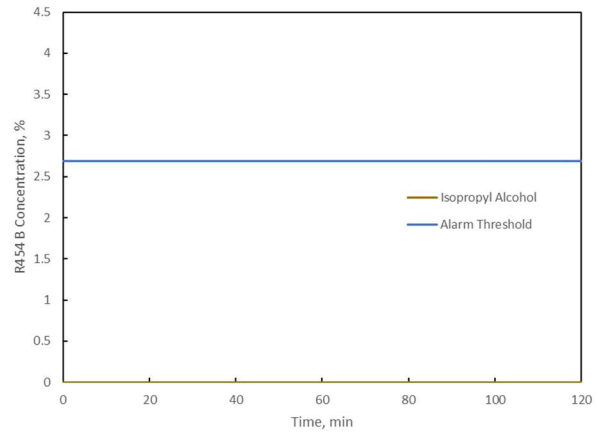

(a) NDIR sensor response

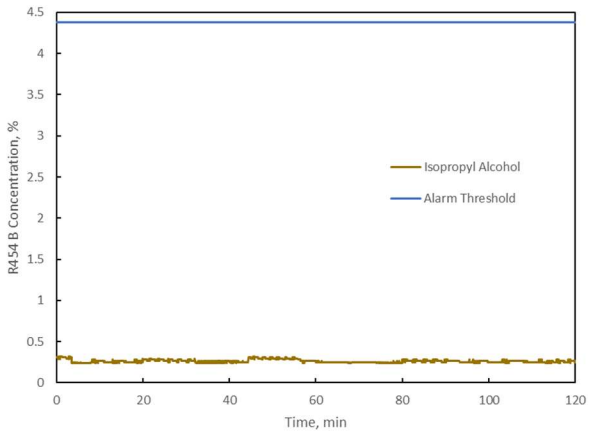

(b) SS response

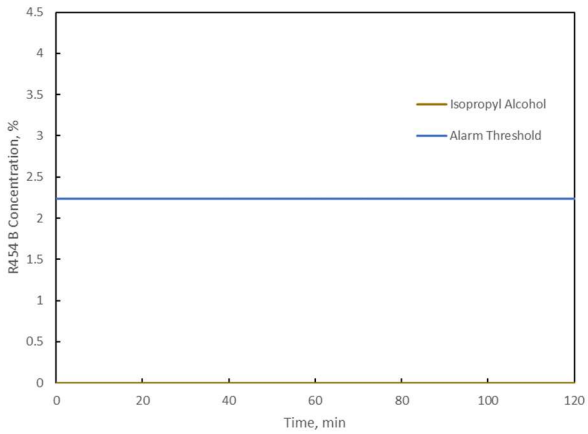

(c) MPS sensor response

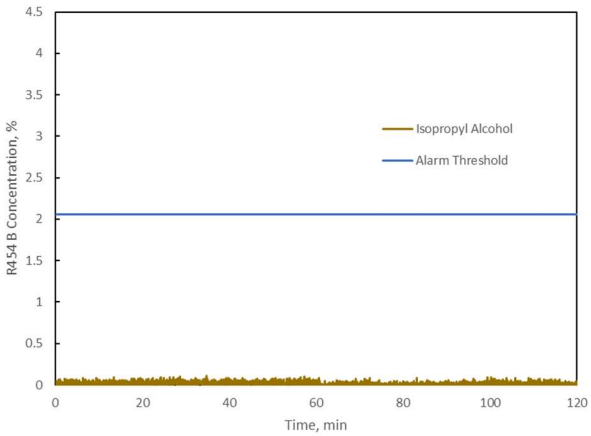

(d) Thermal conductivity sensor response

Figure 4.6. Results of isopropyl alcohol contamination on (a) NDIR, (b) SS, (c) MPS, and (d) thermal conductivity sensor.

Figure 4.6 shows the sensor response to isopropyl alcohol contamination. The NDIR sensor shows no response to the contaminating chemical. This indicates that the UL standard 60335-2-40 specified concentration of isopropyl alcohol does not influence the NDIR sensor output. The SS, thermal conductivity, and MPS sensors do not show a change in their baseline output.

Carbon Dioxide

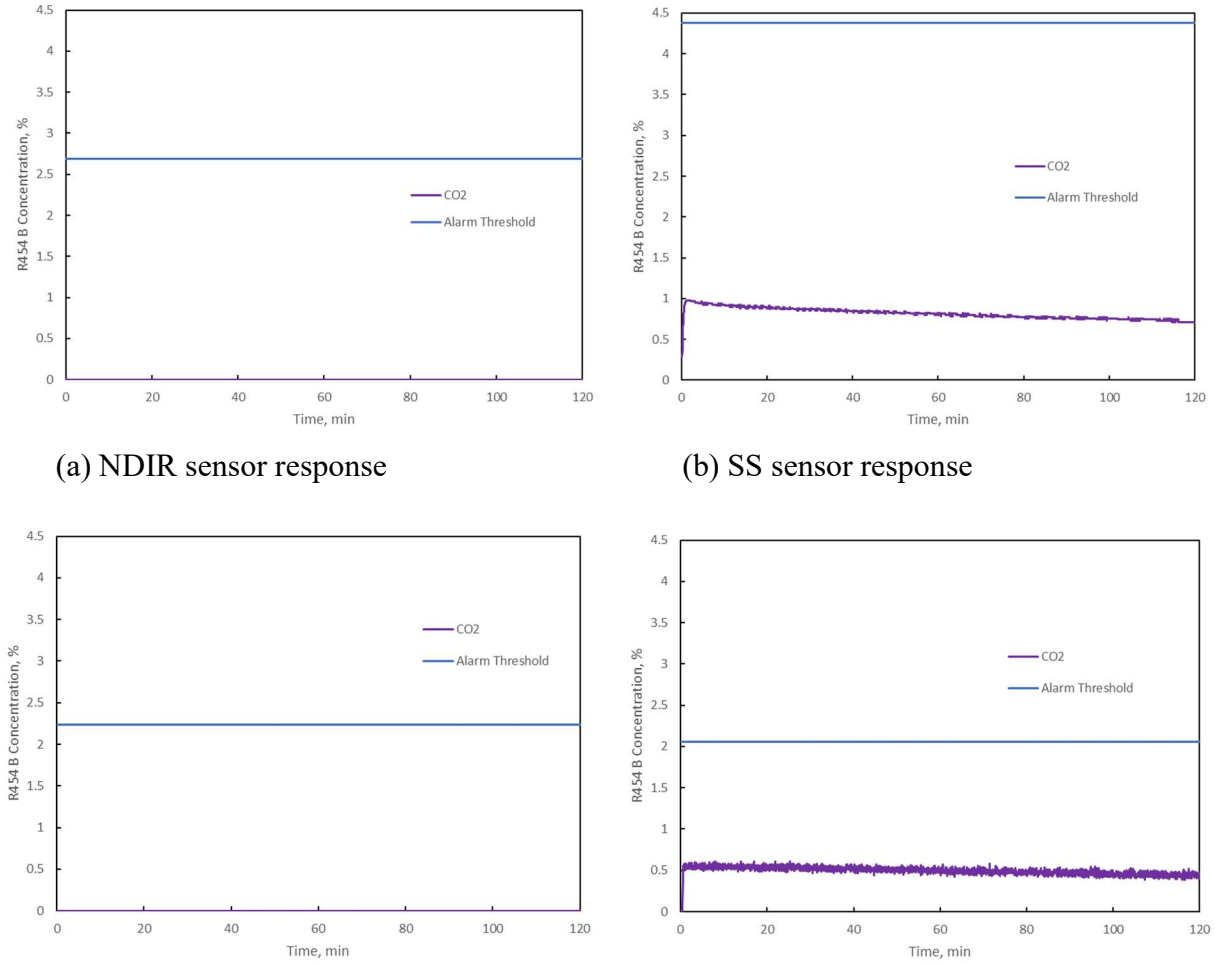

(a) NDIR sensor response

(b) SS sensor response

(c) MPS sensor response

(d) Thermal conductivity sensor response

Figure 4.7. Results of carbon dioxide contamination on (a) NDIR, (b) SS, (c) MPS, and (d) thermal conductivity sensor.

Figure 4.7 shows the sensor response to carbon dioxide contamination. The NDIR sensor shows no response to the contaminating chemical. This indicates that the UL standard 60335-2-40 specified concentration of carbon dioxide does not influence the NDIR sensor output. The SS and thermal conductivity sensors did show a change in their baseline output. The SS sensor increased from 2% LFL to about 7% LFL output. This is not close to the 25% threshold of 31.3% LFL. The thermal conductivity sensor increased from 0% concentration to a steady state output of 0.6% concentration. This is not above the 25% LFL threshold of 2.06% and would trigger a false alarm.

Ammonia

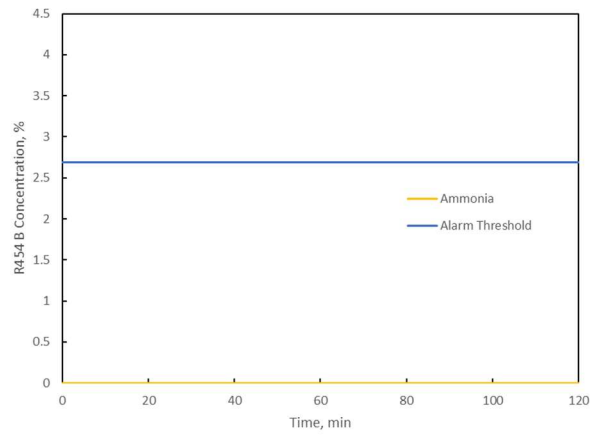

(a) NDIR sensor response

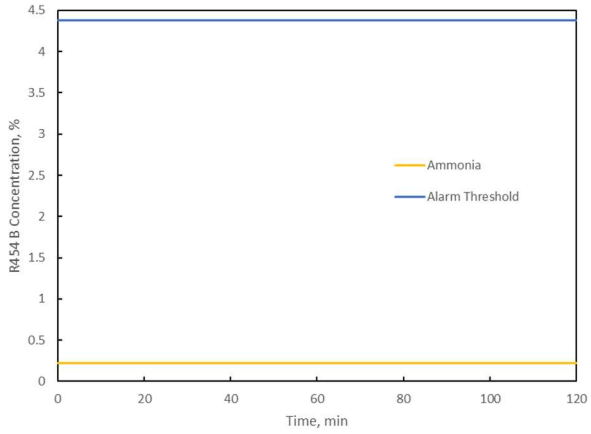

(b) SS response

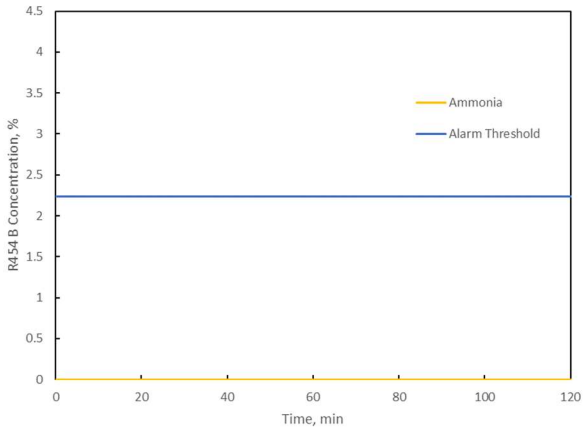

(c) MPS sensor response

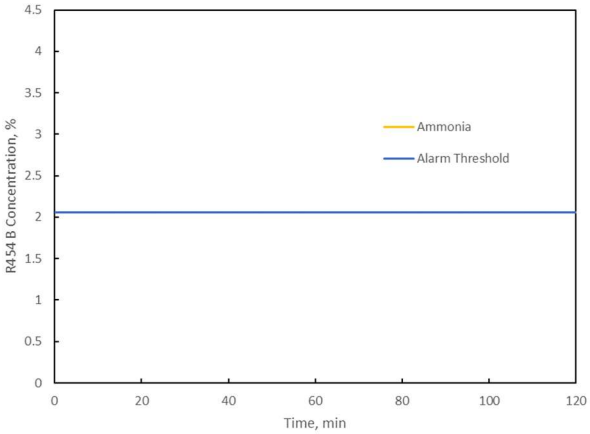

(d) Thermal conductivity sensor response

Figure 4.8. Results of ammonia contamination on (a) NDIR, (b) SS, (c) MPS, and (d) thermal conductivity sensor.

Figure 4.8 shows the sensor response to ammonia contamination. The NDIR sensor shows no response to the contaminating chemical. This indicates that the UL standard 60335-2-40 specified concentration of ammonia does not influence the NDIR sensor output. The SS, MPS, and thermal conductivity sensors did not show a change in their baseline output.

Ethanol

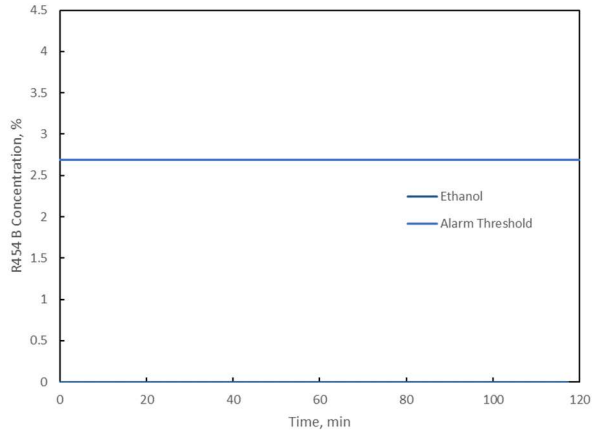

(a) NDIR sensor response

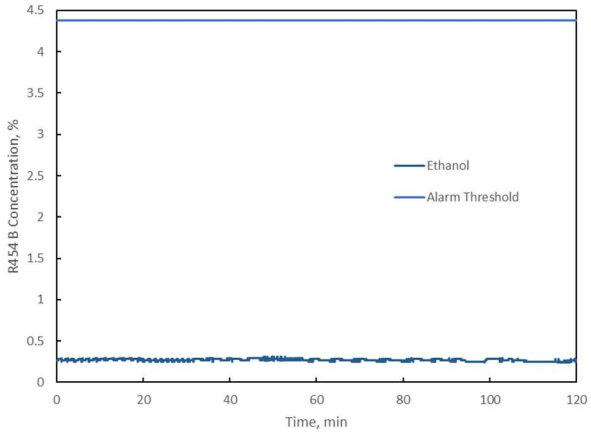

(b) SS response

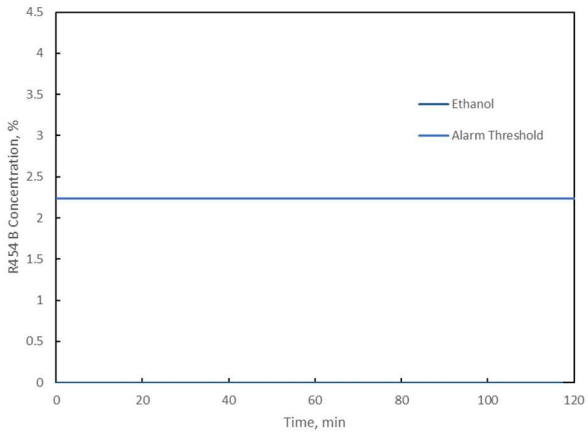

(c) MPS sensor response

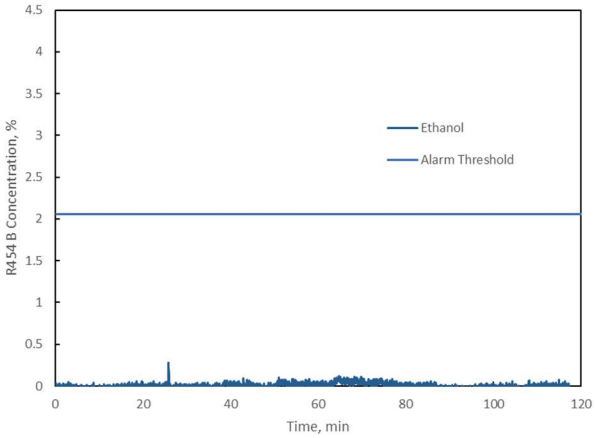

(d) Thermal conductivity sensor response

Figure 4.9. Results of ethanol contamination on (a) NDIR, (b) SS, (c) MPS, and (d) thermal conductivity sensor.

Figure 4.9 shows the sensor response to ethanol contamination. The NDIR sensor shows no response to the contaminating chemical. This indicates that the UL standard 60335-2-40 specified concentration of ethanol does not influence the NDIR sensor output. The SS, MPS, and thermal conductivity sensors did not show a change in their baseline output.

Toluene

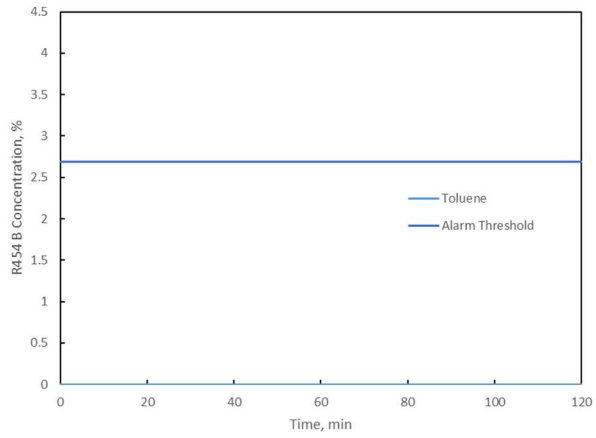

(a) NDIR sensor response

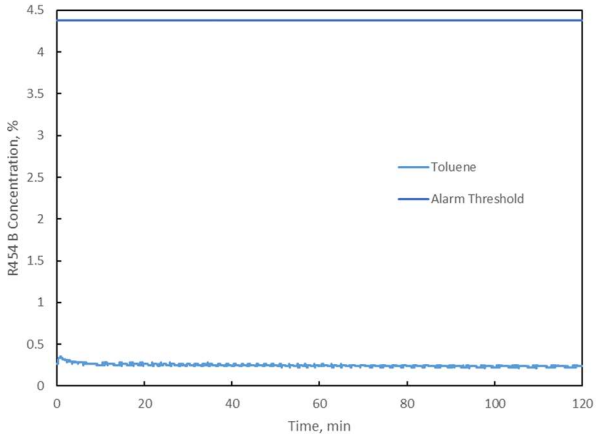

(b) SS response

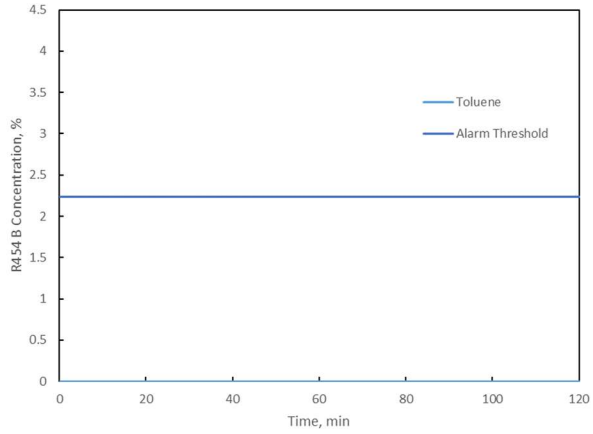

(c) MPS sensor response

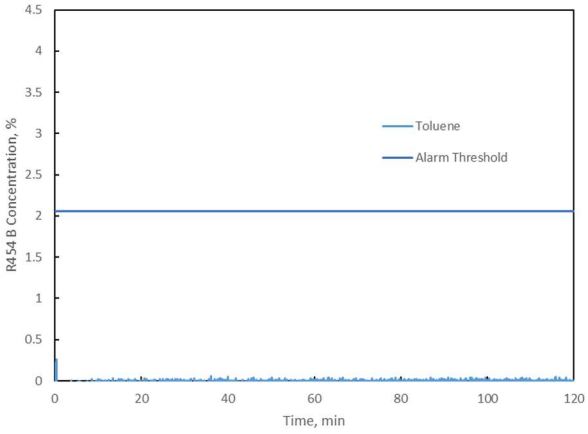

(d) Thermal conductivity sensor response

Figure 4.10. Results of toluene on (a) NDIR, (b) SS, (c) MPS, and (d) thermal conductivity sensor.

Figure 4.10 shows the sensor response to toluene contamination. The NDIR sensor shows no response to the contaminating chemical. This indicates that the UL standard 60335-2-40 specified concentration of toluene does not influence the NDIR sensor output. The SS, MPS, and thermal conductivity sensors did not show a change in their baseline output.

Trichloroethane

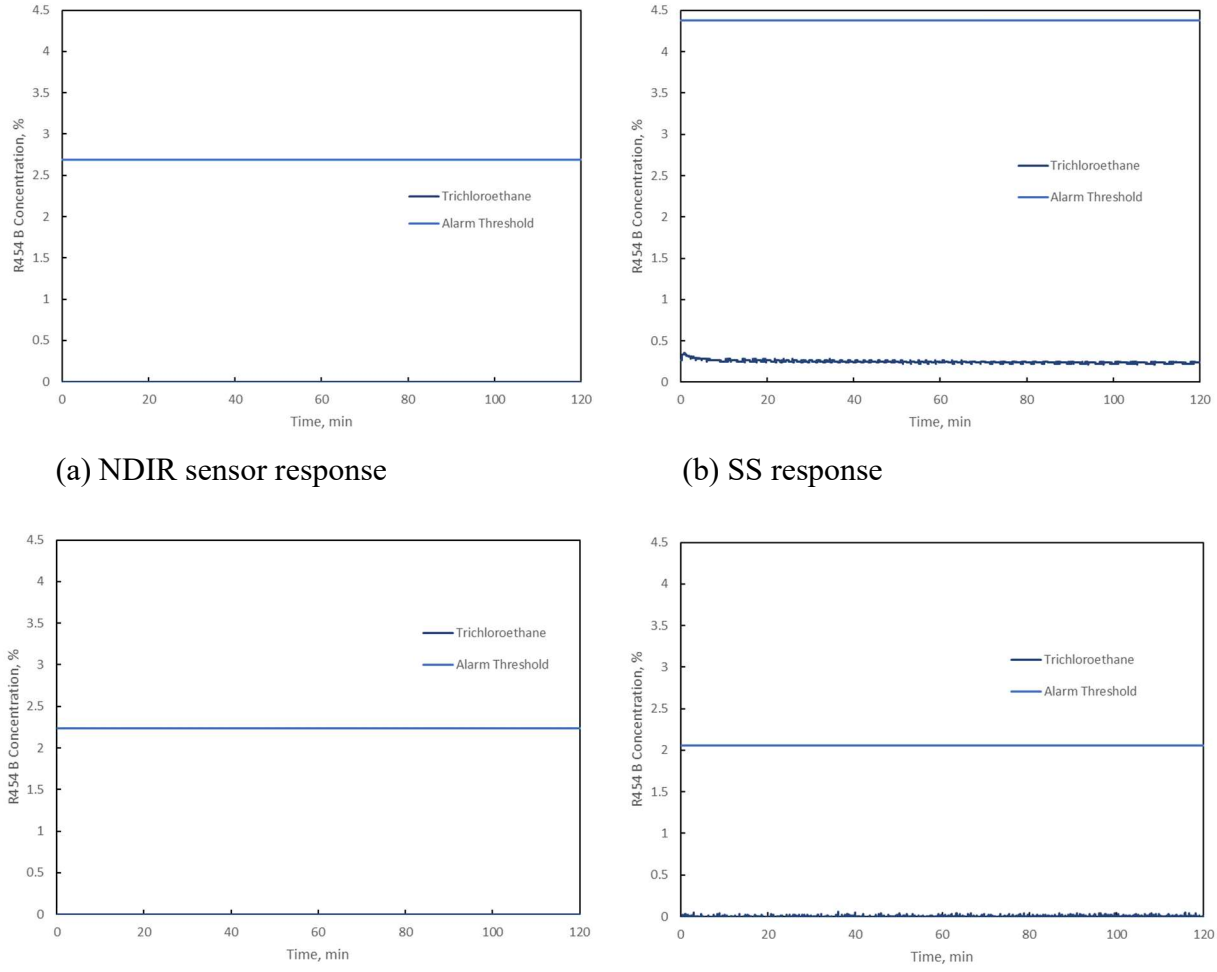

(a) NDIR sensor response (b) SS response

(c) MPS sensor response (d) Thermal conductivity sensor response

Figure 4.11. Results of trichloroethane on (a) NDIR, (b) SS, (c) MPS, and (d) thermal conductivity sensor.

Figure 4.11 shows the sensor response to trichloroethane contamination. The NDIR sensor shows no response to the contaminating chemical. This indicates that the UL standard 60335-2-40 specified concentration of trichloroethane does not influence the NDIR sensor output. The SS, MPS, and thermal conductivity sensors did not show a change in their baseline output.

Acetone

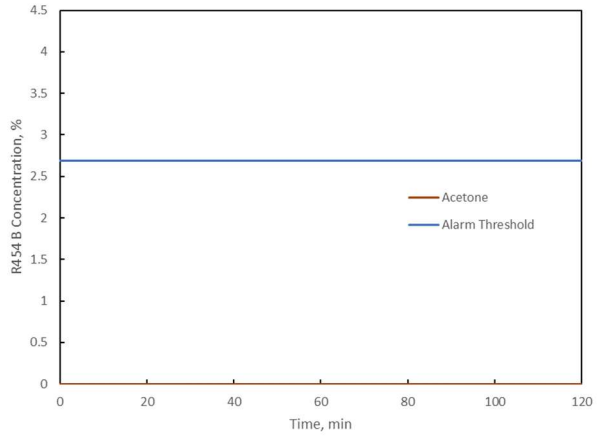

(a) NDIR sensor response

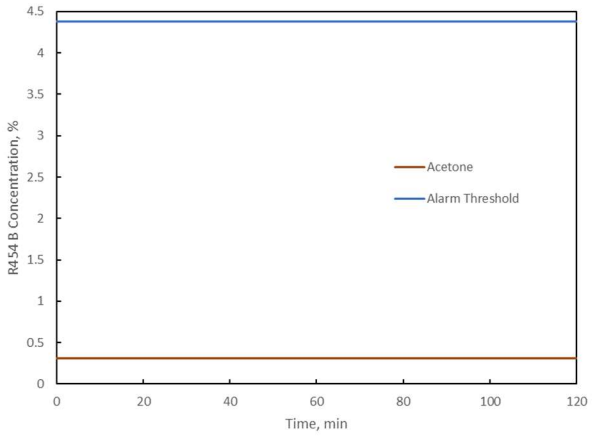

(b) SS response

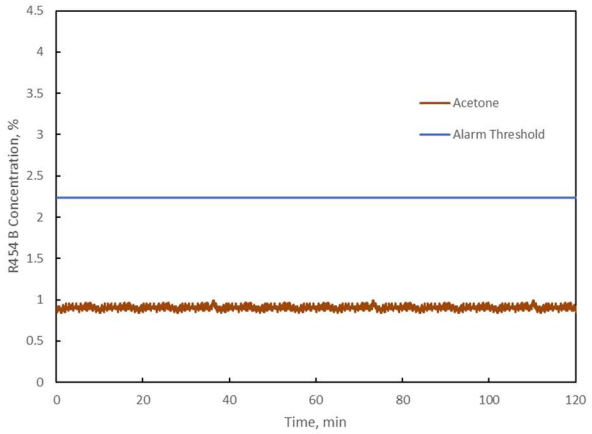

(c) MPS sensor response

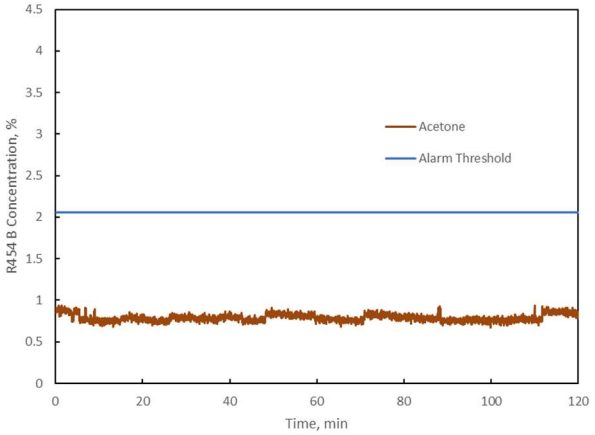

(d) Thermal conductivity sensor response

Figure 4.12. Results of acetone on (a) NDIR, (b) SS, (c) MPS, and (d) thermal conductivity sensor.

Figure 4.12 shows the sensor response to acetone contamination. The NDIR sensor shows no response to the contaminating chemical. This indicates that the UL standard 60335-2-40 specified

concentration of acetone does not influence the NDIR sensor output. The SS sensor did not show a change in base output. The MPS and thermal conductivity sensors did show a change in their baseline output. The MPS sensor had an increase from 0% LFL to about 6% LFL. This was not near the 25% LFL threshold of 15.7%. The thermal conductivity sensor had an increase from 0% concentration to 0.8% concentration. This was not near the 25% LFL threshold of 2.06%.

Decamethylcyclopentasiloxane

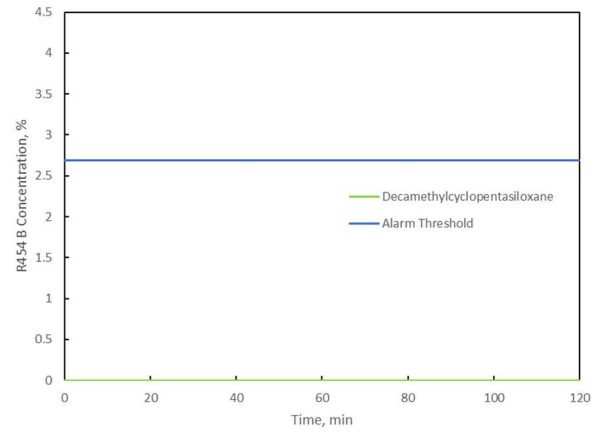

(a) NDIR sensor response

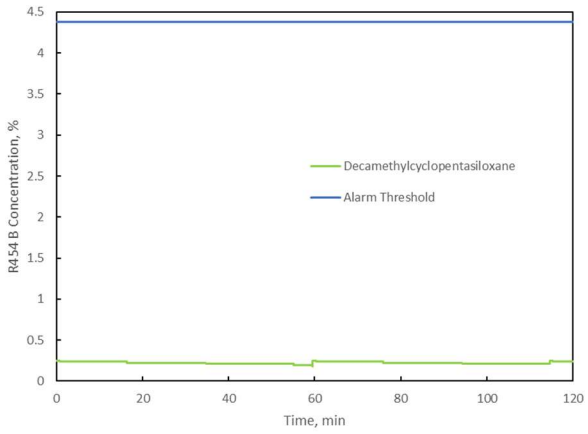

(b) SS response

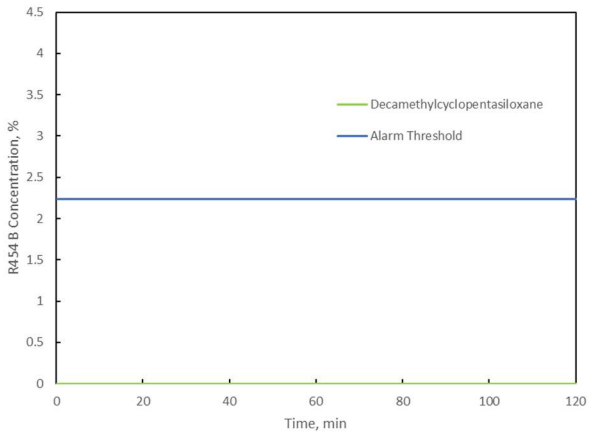

(c) MPS sensor response

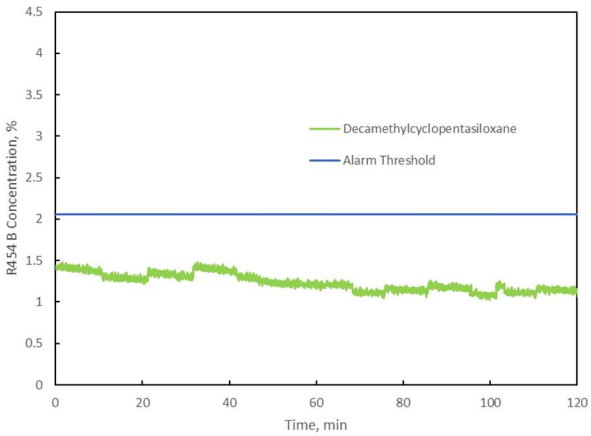

(d) Thermal conductivity sensor response

Figure 4.13. Results of decamethylcyclopentasiloxane on (a) NDIR, (b) SS, (c) MPS, and (d) thermal conductivity sensor.

Figure 4.13 shows the sensor response to decamethylcyclopentasiloxane contamination. The NDIR sensor shows no response to the contaminating chemical. This indicates that the UL standard 60335-2-40 specified concentration of decamethylcyclopentasiloxane does not influence the NDIR sensor output. The SS sensor and MPS sensor did not show a change in base output. The thermal conductivity sensor did show a change in their baseline output. The thermal conductivity sensor had an increase from 0% concentration to steady state output around 1.2% concentration. This was not near the 25% LFL threshold of 2.06%.

Octamethylcyclotetrasiloxane

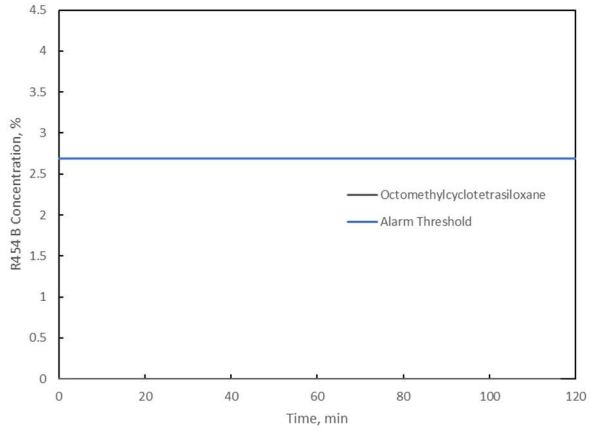

(a) NDIR sensor response

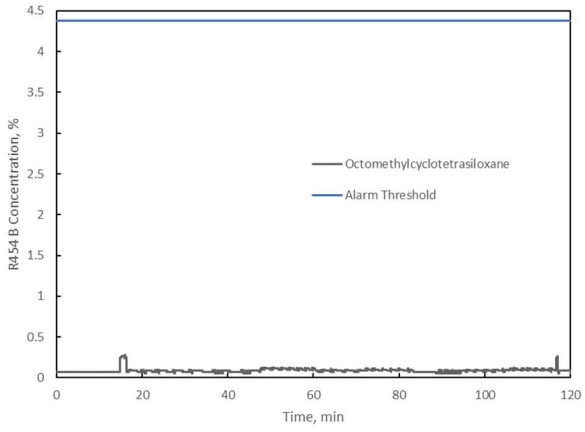

(b) SS response

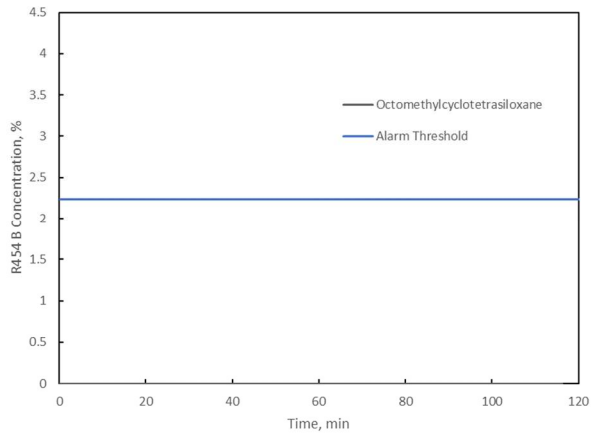

(c) MPS sensor response

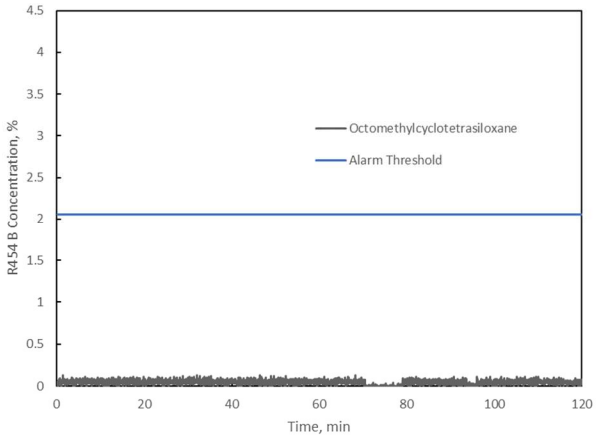

(d) Thermal conductivity sensor response

Figure 4.14. Results of octamethylcyclotetrasiloxane on (a) NDIR, (b) SS, (c) MPS, and (d) thermal conductivity sensor.

Figure 4.14 shows the sensor response to octamethylcyclotetrasiloxane contamination. The NDIR sensor shows no response to the contaminating chemical. This indicates that the UL standard 60335-2-40 specified concentration of octamethylcyclotetrasiloxane does not influence the NDIR sensor output. The SS, thermal conductivity, and MPS sensor did not show a change in base output.

State of Health

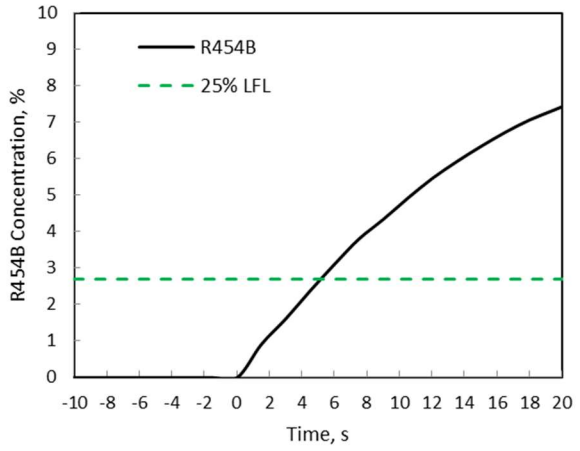

(a) NDIR sensor response

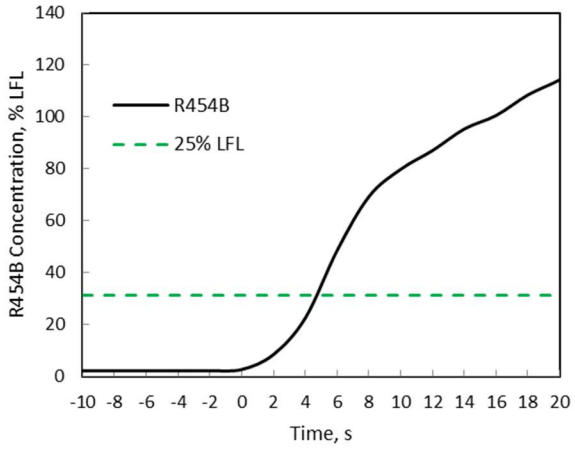

(b) SS response

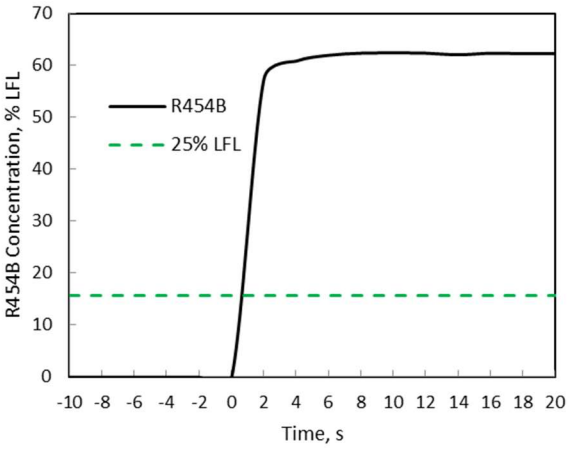

(c) MPS sensor response

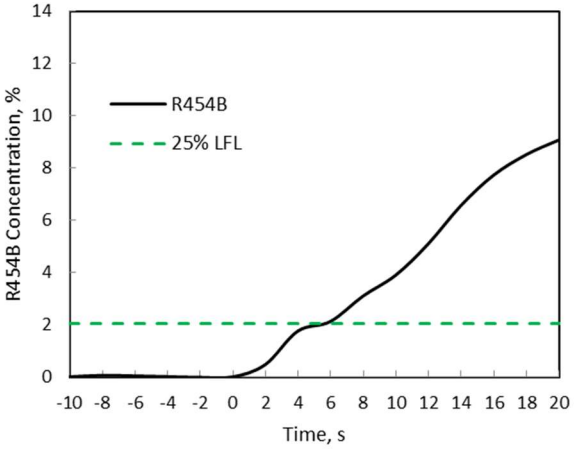

(d) Thermal conductivity sensor response

Figure 4.15. Results from R-454B state of health test on (a) NDIR, (b) SS, (c) MPS, and (d) thermal conductivity sensor.

Figure 4.15 shows the results from the state of health tests performed after exposing the sensor to each of the contaminants. The NDIR sensor had a response time of 5 seconds post contamination. The SS sensor had a response time of 5 seconds. The MPS sensor had a response time of 1 second. The thermal conductivity sensor had a response time of 6 seconds.

4.6 Discussion of Results

Table 4.5 summarizes the results of the contamination tests for the NDIR sensor. The NDIR sensor showed no increase in output when exposed to any of the contaminants. The state of health test showed that the sensor had a response time of 5 seconds which is the exact same response time the sensor had before any of the contamination trials.

Table 4.5. Summary from contamination and state of health tests.

Contaminant	NDIR Increase in Output (Y/N)	SS Increase in Output (Y/N)	TC Increase in Output (Y/N)	MPS Increase in Output (Y/N)
Methane	N	N	N	N
n-Butane	N	N	N	N
n-Heptane	N	N	N	N
Ethyl Acetate	N	N	Y	N
Isopropyl Alcohol	N	N	N	N
Carbon Dioxide	N	Y	Y	N
Ammonia	N	N	N	N
Ethanol	N	N	N	N
Toluene	N	N	N	N
Trichloroethane	N	N	N	N
Acetone	N	N	Y	Y
Decamethylcyclopentasiloxane	N	N	Y	N
Octamethylcyclotetrasiloxane	N	N	N	N

Table 4.5 summarizes the results of the SS sensor. This sensor showed no response to any of the contaminants except for carbon dioxide. The increase in output was minimal. The output only increased by about 4% LFL which is not close to the 25% LFL threshold of 31.3% LFL for this sensor. The sensor returned to its baseline reading for the rest of the contamination tests. The state of health test showed that the sensor response time had decreased from 7 seconds to 5 seconds after all the contamination tests. While this response time is still within the limit set by the UL 60335-2-40 standard, it does indicate that the contamination tests had a slight poisoning effect on the sensor.

Table 4.5 summarizes the contamination results for the MPS sensor. This sensor only showed a response to acetone. The output increased from 0% LFL to about 6% LFL. This was not close to the 25% LFL threshold which was 27% LFL for this sensor. The state of health test for this sensor indicated that the contaminants had no effect on the sensor response time. Both before and after contamination testing, the response time for the MPS sensor was 1 second

Table 4.5 summarizes the contamination results for the thermal conductivity sensor. This sensor showed an increase in output for ethyl acetate, carbon dioxide, acetone, and for decamethylcyclopentasiloxane, however none of the contaminants caused the sensor's output to increase above the 25% LFL threshold. The 25% LFL threshold for this sensor was 2.06%. The response time of the sensor before contamination was 7 seconds. The state of health post contamination tests showed that the sensor had a response time of 6 seconds. Even though the sensor response time improved, the change in sensor response post contamination does indicate the exposure to contamination did have an effect on the sensor's output.

Chapter 5: Conclusions and Future Work

Due to recent changes in state legislation, old refrigerant gasses are being phased out to be replaced by A2L refrigerants which have a lower GWP but are mildly flammable. This flammability hazard needs to be addressed in a way that can notify an occupant that the concentration of refrigerant is within the LFL. The solution to this hazard is A2L refrigerant area monitoring detection systems. This study's objectives were to determine an available sensing technology and a corresponding sensor available for purchase, construct an apparatus to test with this sensor, determine the sensors response time to A2L class refrigerants, R-32 and R-454B, and determine the sensors response to contaminants and contaminant effect on sensor health.

An A2L refrigerant sensor using NDIR technology was identified and selected to characterize its response to A2L refrigerants R-454B and R-32. Sensors using MPS, SS, and thermal conductivity technologies were also tested in tandem with the NDIR sensor to compare results. A test apparatus was constructed based on a modified version of Wack's [10] test apparatus. Calibrated rotameters were used to measure how much of each gas was needed to dilute the refrigerants to the desired concentrations. The response times were measured in accordance with the UL 60335-2-40 standard [7] by first obtaining the steady state output of the sensor in 25% of the LFL and then plunging the sensor into 100% of the LFL and measuring the time it takes the output to cross the 25% LFL steady state output. Annex LL of this standard requires that the response time of the sensor must be under 10 seconds [7]. The sensors were also tested with a prescribed list of contaminants and corresponding concentrations also provided by the UL 60335-2-40 standard. These contaminants were thought to be chemicals that could be commonly found inside a residential application and could come into contact with the sensor. Some of these

chemicals were obtained as gasses and were diluted the same way the refrigerants were, and some were obtained as liquids and required nitrogen to be bubbled through them to obtain the liquid chemical's vapors. Each of the sensors were exposed to the contaminants one contaminant at a time for 2 hours at a time. The sensors were allowed 16 hours of recovery before being tested with the next contaminant. Following these contamination tests, a state of health test was conducted on the sensors in accordance with Section LL.3DV of the UL 60335-2-40 standard [7]. This state of health test was another response time test.

The NDIR sensor was able to meet the 10 second requirement when plunged into 100% of the refrigerant LFL. The NDIR sensor was second fastest with a response time of 5 seconds. The SS sensor, MPS sensor, and thermal conductivity sensor also tested in accordance with the UL 60335-2-40 standard were able to meet the 10 second requirement. The SS sensor had a response time of 7 seconds, the MPS sensor had a response time of 1 second, and the thermal conductivity sensor had a response time of 7 seconds. The NDIR sensor showed no response to any of the 13 exposures to contaminants. The SS sensor and the MPS sensor each showed an increase in output for 1 out of the 13 contaminants used, but the increase in output was negligible and would not have crossed the 25% steady state threshold. The thermal conductivity sensor showed an increase in output for 4 out of the 13 contaminants. However, none of the contaminants caused the sensor output to cross the 25% LFL threshold causing a false alarm. The NDIR sensor showed a response time of 5 seconds, which did not change from the response time before the contamination tests. The MPS sensor also showed a response time of 1 second which did not change from before the contamination tests. The SS sensor and thermal conductivity sensor each had a different response time after being exposed to the contaminants. The SS sensor had a response time of 5 seconds after contamination tests which was 2 seconds faster than the response time before exposure to

contamination. The thermal conductivity sensor had a response time of 6 seconds which was 1 second faster than the response time before exposure to contamination. Based on the results from the contamination and the response time tests before and after contamination, the NDIR sensor has shown to have the best performance out of the 4 technologies tested and is recommended for area monitoring leak detection for A2L refrigerants. It had the second fastest pre-contamination response time and was consistent before and after contamination. The sensor also had no change in output when exposed to any contaminant. This indicates that the health of the NDIR sensor was not affected by the contaminants. The MPS sensor performed the second best and is a viable alternative to the NDIR sensor for area monitoring leak detection. It had the fastest response time and was consistent before and after contamination, but it did have a change in output in response to one of the contaminants. The thermal conductivity and SS sensor are not recommended for area monitoring leak detection for A2L refrigerants. The thermal conductivity sensor responded to 4 of the 13 contaminants. Both sensors also had a response time that was under 10 seconds but was not consistent before and after contamination.

For future testing, more experiments could be done to better characterize the NDIR sensor response to A2L refrigerants and the UL 60335-2-40 list of contaminants. The sensor is meant to be employed over years of service. Repeated exposures to refrigerants over the course of a year should be done to observe if repeated exposures can have any long-term effect on the sensor health. Another output that could be characterized is long term exposure. The sensor could be exposed to a concentration of the refrigerant that does not cause the alarm to trigger for a prolonged amount of time. Trials that last 24 hours or longer could be done to see if continuous low concentration exposure could affect the sensor's health. These types of results could be included into the UL 60335-2-40 standard by adding a section that would trigger an alarm if the original baseline output

of the sensor has changed for 24 hours. This study used R-454B and R-32 to characterize the sensor's original response. However, more A2L refrigerants will be used as the transition to use refrigerants with lower GWP happens. The response to all the potential commercial A2L refrigerants should be characterized to understand the sensor's response to different A2L refrigerants. When the sensors were exposed to the contaminants, they were exposed one at a time with 16-hour intervals in between tests. However, in a residential application, it is likely that a contaminant may be exposed to the sensor at the same time a refrigerant leak occurs. An improvement to characterizing the sensor response to contamination would be to perform a response time test with a gas mixture including both 100% of the refrigerant LFL and the prescribed concentration of contaminant to see how the contaminant directly interferes with the sensor response time.

Since the market for these sensors are still in development, other types of sensing technologies are currently being utilized to do the same work done in this study. Other sensing technologies than the ones used for this study should be considered and tested as they emerge on the market to compare sensor performances. The MPS sensor showed it was a viable alternative to the NDIR sensing technology. More studies like the ones previously described should be done with sensors utilizing the MPS technology to better characterize the technologies response to A2L refrigerants.

Bibliography

[1] IPCC. Changes in Atmospheric Constituents and in Radiative Forcing. Climate Change 2007: The Physical Science Basis, 212, 2007.

[2] FETA. An Introduction to A2L Refrigerants and Their Use in Refrigeration, Air Conditioning and Heat Pump applications. Technical report, Federation of Environmental Trade Associations, 2017.

[3] ASHRAE. Standard 34-2013, Designation and Safety Classification of Refrigerants. Technical report, American Society of Heating, Refrigerating and Airconditioning Engineers, Atlanta, 2013.

[4] H. Pham and R. Rajendran. R32 And HFOs As Low-GWP Refrigerants For Air Conditioning. International Refrigeration and Air Conditioning Conference, Paper 1235, 2012.

[5] M. Wagner and R. Ferenchiak. Leak Detection of A2L Refrigerants in HVACR Equipment. Technical report, Air-Conditioning, Heating and Refrigeration Technology Institute, 2017.

[6] M. Smith. California Refrigerant Regulations Overview. Technical report, North American Sustainable Refrigeration Council, 2019.

[7] UL. Standard 60335-2-40. Household And Similar Electrical Appliances – Safety – Part 2-40: Particular Requirements for Electrical Heat Pumps, Air-Conditioners and Dehumidifiers. Technical report, Underwriters Laboratory, 2019.

[8] D. McClure and T. Anderson. A Comparison of Refrigerant Constant Monitoring Leak Detectors. International Refrigeration and Air Conditioning Conference, Paper 115, 1990.

[9] R. Tapscott and C. Sohn. Halocarbon Refrigerant Detection Methods. Technical report, US Army Construction Engineering Research Laboratories, Champaign, Illinois, 1996.

[10] Sunderland, Peter B, and Wack, Garrett James. “Characterization of Metal-Oxide Semiconductor Sensors for R-32 and R-454b Leaks.” University of Maryland (College Park, Md.), 2020.

[11] Danfoss. Application Guide for Gas Detection in Refrigeration Systems, 2007.

[12] Microelectro Mechanical Systems & MEMS sensors. NevadaNano. (2022, May 16). Retrieved June 23, 2022, from https://nevadanano.com/our-technology/#:~:text=We%20call%20it%20the%20Molecular,rich%20dataset%20of%20chemical%20information

[13] P. Sudhakar, P. Latha, P.V. Reddy, Chapter 17 - Analytical techniques, Editor(s): P. Sudhakar, P. Latha, P.V. Reddy, Phenotyping Crop Plants for Physiological and Biochemical Traits, Academic Press, 2016, Pages 137-149, ISBN 9780128040737, https://doi.org/10.1016/B978-0-12-804073-7.00017-X

[14] Keeratirawee, Kanchalar, and Peter C Hauser. “Determination of Binary Gas Mixtures by Measuring the Resonance Frequency in a Piezoelectric Tube.” Sensors (Basel, Switzerland) vol. 22,4 1691. 21 Feb. 2022, doi:10.3390/s22041691

[15] Lee, H.-J., Kang, B.-H., Han, S.-H., Kim, D.-E., Kown, D.-H., & Kang, S.-W. (2005). Non-invasive optical transcutaneous pCO2 monitoring system based on NDIR method . In ICST 2005: Proceedings of the first international conference on sensing technology: Massey University, Palmerston North, New Zealand, November 21-23, 2005 (pp. 292–296). Palmerston North, N.Z.; Institute of Information Sciences and Technology, Massey University.

[16] Jongwon Kwon, Gwanghoon Ahn, Gyusik Kim, J. C. Kim and Hiesik Kim, "A study on NDIR-based CO2 sensor to apply remote air quality monitoring system," 2009 ICCAS-SICE, 2009, pp. 1683-1687.

[17] Trieu-Vuong Dinh, In-Young Choi, Youn-Suk Son, Jo-Chun Kim, A review on non-dispersive infrared gas sensors: Improvement of sensor detection limit and interference correction, Sensors and Actuators B: Chemical, Volume 231, 2016, Pages 529-538, ISSN 0925-4005, https://doi.org/10.1016/j.snb.2016.03.040.

[18] Adam Sklorz, Steffen Janßen, Walter Lang, Detection limit improvement for NDIR ethylene gas detectors using passive approaches, Sensors and Actuators B: Chemical, Volume 175, 2012, Pages 246-254, ISSN 0925-4005, https://doi.org/10.1016/j.snb.2012.09.085.

[19] Yang Jing, Cheng Yuhua, Yuan Yupeng, Li Xiaofei, Zhang Zuwei, Xu Ming, Wang Dengpan, Mu Jiangdong, Mei Yong, Zhang Yuzhe, Design and optimization of an integrated MEMS gas chamber with high transmissivity, Digital Communications and Networks, Volume 7, Issue 1, 2021, Pages 82-91, ISSN 2352-8648, https://doi.org/10.1016/j.dcan.2020.05.006.

[20] Hehuan Liu, Yunbo Shi, and Tian Wang, "Design of a six-gas NDIR gas sensor using an integrated optical gas chamber," Opt. Express 28, 11451-11462 (2020)

[21] Cubic R32 A2L refrigerant sensor. Gaslab.com. (2022). Retrieved June 23, 2022, from https://gaslab.com/products/a2l-refrigerant-sensor-cubic-am4205

[22] Cubic R32 A2L refrigerant sensor. Gaslab.com. (2022). Retrieved June 23, 2022, from https://gaslab.com/products/a2l-refrigerant-sensor-cubic-am4205

[23] U. Nanda and S. K. Pattnaik, "Universal Asynchronous Receiver and Transmitter (UART)," 2016 3rd International Conference on Advanced Computing and Communication Systems (ICACCS), 2016, pp. 1-5, doi: 10.1109/ICACCS.2016.7586376.

[24] [19] Difluoromethane; SDS No.: 000010021734 [Online]; Linde Gas GmbH: Carl-von-Linde-Platz 1, Austria, Nov 26, 2018.

[25] [20] R-454B; SDS No.: 1354822-00035 [Online]; Chemours: Baanhoekweg 22, Netherlands, Dec 1, 2017.